The role of geomagnetic field intensity in late Quaternary evolution of humans and large mammals

J.E.T. Channell[1] and L. Vigliotti[2]

[1] Department of Geological Sciences, University of Florida, Gainesville, FL 32611, USA

[2] Istituto di Scienze Marine, ISMAR-CNR, Via P. Gobetti 101, 40129 Bologna, Italy

Corresponding author: James E.T. Channell (jetc@ufl.edu)

Key Points: (1) The strength of the geomagnetic field is a proxy for the flux of ultra-violet radiation (UVR). (2) The disappearances of the Neanderthals and many large mammals during the Late Quaternary occur during minima in geomagnetic field strength. (3) Human phylogeny from mitochrondrial DNA and Y-chromosomes can also be linked to minima in field strength, hence UVR flux.

Abstract

It has long been speculated that biological evolution was influenced by ultra-violet radiation (UVR) reaching the Earth's surface, despite imprecise knowledge of the timing of both UVR flux and evolutionary events. The past strength of Earth's dipole field provides a proxy for UVR flux because of its role in maintaining stratospheric ozone. The timing of Quaternary evolutionary events has become better constrained by fossil finds, improved radiometric dating, use of dung fungi as proxies for herbivore populations, and improved ages for nodes in human phylogeny from human mitochrondrial DNA (mtDNA) and Y-chromosomes. The demise of Neanderthals at ~41 ka can now be closely tied to the intensity minimum associated with the Laschamp magnetic excursion, and the survival of anatomically modern humans (AMHs) can be attributed to differences in the aryl hydrocarbon receptor (AhR) that has a key role in the evolutionary response to UVR flux. Fossil occurrences and dung-fungal proxies in Australia indicate that episodes of Late Quaternary extinction (LQE) of mammalian megafauna occurred close to the Laschamp and Blake magnetic excursions. Fossil and dung fungal evidence for the age of the LQE in North America (and Europe) coincide with a prominent decline in geomagnetic field intensity at ~13 ka. Over the last ~200 kyr, phylogeny based on mtDNA and Y-chromosomes in modern humans yield nodes and bifurcations in evolution corresponding to geomagnetic intensity minima which supports the proposition that UVR reaching Earth's surface influenced mammalian evolution with the loci of extinction controlled by the geometry of stratospheric ozone depletion.

Plain Language Summary

The strength of Earth's magnetic field in the past, recorded by rocks and sediments, provides a proxy for past flux of ultra-violet radiation (UVR) to Earth's surface due to the role of the field in modulating stratigraphic ozone. About 40 thousand years ago, mammalian fossils in Australia and Eurasia record an important die-off of large mammals that included Neanderthals in Europe. In the Americas and Europe, a large

mammal die-off appears to have occurred ~13 thousand years ago. Both die-offs can be linked to minima in Earth's magnetic field strength implying that UVR flux variations to Earth's surface influenced mammalian evolution. For the last ~200 thousand years, estimates of the timing of branching episodes in the human evolutionary tree, from modern and fossil DNA and Y-chromosomes, can be linked to minima in field strength which implies a long-term role for UVR in human evolution. New fossil finds, improved fossil dating, knowledge of the past strength of Earth's magnetic field, and refinements in the human evolutionary tree, are sharpening the focus on a possible link between UVR arriving at the Earth's surface, magnetic field strength, and events in mammalian evolution.

Index Terms: Paleointensity (1521), Evolutionary Geobiology (0444), Macropaleontology (0459)

1. Introduction

The apparent spacing of mass extinction events at long (~26 Ma*) repeat times (e.g., Raup & Sepkoski, 1986), and the supposed role of geomagnetic polarity reversal in extinction (e.g., Raup, 1985), have received intermittent attention over the last 50 years, since early studies of Quaternary radiolarian evolution and polarity reversal in deep-sea sediments (Hays, 1971). These efforts have not resulted in significant traction for claims of a linkage between polarity reversal (with its concomitant low field intensity) and extinction or speciation, perhaps because of uncertainties in the polarity timescale itself, and in the chronology of extinction/speciation outside of the few well-documented mass extinctions. On the other hand, we now know from Quaternary studies that although polarity reversals coincided with relative paleointensity (RPI) minima, intervals between polarity reversals are also characterized by numerous RPI minima, some of which coincide with magnetic excursions (see Laj & Channell, 2015). The chronology of both the RPI record and the paleontological record remains poorly constrained, even for the Quaternary, such that a linkage between extinction and RPI minima cannot be ruled out.

The geomagnetic field helps to preserve stratospheric ozone, as well as atmospheric composition, density and oxygen levels that are vital to Earth's biosphere (Wei et al., 2014). The field shields Earth from galactic cosmic rays (GCR) and solar wind, and from harmful ultraviolet radiation (UVR) that affect the function of living systems (Belisheva et al., 2012; Mendoza & de la Pena, 2010). The demise of the Martian magnetic field, several billion years ago, is widely believed to have been the root cause for the near disappearance of the Martian atmosphere and the resulting dramatic change in the Martian environment from one featuring surface water and aqueous sedimentation to its present relative inactivity and sterility. The explosion of life in the Early Cambrian period at ~530 Ma has been associated with growth of Earth's inner core, the supposed strengthening of the dipole geomagnetic field, and the resulting thickening of Earth's

* The reader is referred to Aubry et al. (2009) for abbreviations denoting geological time in the past (Ma for millions of years ago, and ka for thousands of years ago) and equivalent durations (Myr and kyr, respectively).

atmosphere (Doglioni et al., 2016), although there is little evidence for strengthening of the geomagnetic field at this time (e.g., Biggin et al., 2015). On the other hand, the Late Ediacaran and Early Cambrian periods (~550 and ~530 Ma, respectively) may have been times of unusually high polarity reversal frequency (Pavlov & Gallet, 2001; Bazhenov et al., 2016), although precise estimates of reversal frequency are elusive due to poorly constrained age control in stratigraphic sections where the reversals were recorded. Meert et al. (2016) proposed that high reversal frequency (up to ~20 reversals/Myr) at this time would have been associated with low geomagnetic field intensity that, therefore, lowered shielding from UVR, which created an evolutionary advantage for burrowing and shelled organisms. These proposals for the role of the geomagnetic field in evolution are controversial partly because of poor knowledge of the state of the geomagnetic field 500-550 million years ago. Oxygenation of the oceans and atmosphere after the Gaskiers glaciation at ~580 Ma (Canfield et al., 2007) may have been the principal driver of the Early Cambrian explosion of life, both through oxygen levels at Earth's surface and increased UVR shielding through enhanced stratospheric ozone concentrations.

Several strategies in modern organisms reflect the evolutionary impact of UVR. Behavioral adaptations to UVR include vertical water-column migration in aquatic organisms, the presence of UVR-screening pigmentation decreasing with water depth, and complete disappearance of pigments for deep-water and cave-dwelling animals (e.g., Hessen, 2008). The red coloration of alpine plankton and the "red sweat" of the hippopotamus (Saikawa et al, 2014) are examples of evolutionary adaptation to high UVR at altitude and at low latitudes, respectively. UVR causes two classes of DNA lesions: cyclobutane pyrimidine dimers (CPDs) and 6-4 photoproducts (6-4 PPs). Both lesions distort DNA structure, introducing bends or kinks and thereby impeding transcription and replication (e.g., Clancy, 2008; Branze & Foiani, 2008). Relatively flexible areas of the DNA double helix are most susceptible to damage. One "hot spot" for UV-induced damage is found within a commonly mutated oncogene TP53 (Benjamin & Ananthaswamy, 2006), which in normal function has an important role in tumor suppression. At low concentrations, reactive oxygen species (ROS) play vital roles during mutagenic activity in response to pathogen attack. Higher concentrations of ROS produced by UVR give rise to oxidative stress where ROS attack DNA bases and the deoxyribosyl backbone of DNA (see MacDavid & Aebisher, 2014). Production of antioxidant enzymes neutralizes ROS, and ROS modulation is controlled by the aryl hydrocarbon receptor (AhR) that plays a key role in mammalian evolution.

The consequences of ionizing radiation associated with GCRs and solar particle events (solar wind) for human health have received attention in recent years in an effort to evaluate the health effects of future space travel outside Earth's protective magnetosphere (e.g., Delp et al., 2016). Earth's atmosphere is opaque to all but the highest energy GCRs, and, together with the geomagnetic field, serves to shield Earth's surface from GCRs. The intensity of UVR arriving at Earth's surface decreases with increasing latitude, and is attenuated by stratospheric ozone (O_3) that acts as a sink for UVR. The geomagnetic field plays an important role in preserving the atmosphere, including stratospheric ozone that would otherwise be stripped away by solar wind and GCRs (Wei et al., 2014). UVR triggers dissociation of oxygen molecules (O_2) into oxygen radicals that combine to form stratospheric ozone that in turn absorbs UVR as it splits into oxygen atoms. Certain ozone-depleting agents (such as nitrogen oxides) are

produced naturally by energetic particle precipitation (EPP) from solar wind, particularly during solar proton events (SPE), and therefore times of low geomagnetic field strength lead to higher ozone depletion (Randall et al., 2005, 2007). Atmospheric modeling implies substantial increases in hydrogen and nitrogen oxide concentrations due to enhanced ionization by GCRs during the Laschamp excursion, with significant decrease in stratospheric ozone particularly at high latitudes (Suter et al., 2014). Modeling of ozone depletion during polarity reversals, based on a geomagnetic field intensity ~10% of the present value, leads to enhanced UVR flux at the Earth's surface, particularly at higher latitudes, that is 3-5 times that resulting from the anthropogenic ozone hole (Winkler et al., 2008; Glassmeier & Vogt, 2010). Prior to anthropogenic emission of ozone-depleting chlorofluorocarbons (CFCs) and halons, EPP at times of low geomagnetic field strength played an important role in ozone depletion. A well-defined nitrate peak, together with a broader ^{10}Be peak, are associated with low field strength at the time of the Laschamp magnetic excursion (~41 ka) in the EPICA-Dome C Antarctic ice core (Traversi et al., 2014), which indicates that geomagnetic shielding played a role in the production of both cosmogenic isotopes (such as ^{10}Be) and ozone-depleting nitrogen compounds. It is noteworthy that bacterial UVR proxies in sediments from Lake Reid (Antarctica) imply more than three times higher UVR flux during part of the last glacial than during the Holocene (Hodgson et al., 2005). UVR exposure affects the early stage of life in modern marine plankton, and plankton-benthos coupling in coastal waters (e.g., Hernandez Moresino et al. 2011). Furthermore, UVR plays a role in photosynthesis (e.g., Hollosy, 2002) and can cause changes in vegetation, and habitat modification.

The aim of this paper is to review the record of geomagnetic field intensity over the last ~300 kyr, and compare this record with the fossil record of extinction in terrestrial mammals (including Neanderthals), and with nodes in hominin phylogeny determined from mitochondrial DNA (mtDNA) and Y chromosomes.

2. The geomagnetic field

Knowledge of the Holocene geomagnetic field (i.e. over the last ~12 kyr) has been based on models built from archaeomagnetic, lava and sediment data (Korte et al., 2011; Pavón-Carrasco et al., 2014; Constable et al., 2016). Beyond the Holocene, geomagnetic field strength during the Quaternary, over the last ~2.5 Myr, has been acquired primarily from relative paleointensity (RPI) data from marine sediments recovered by deep-sea drilling (e.g., Laj et al., 2000, 2004; Valet et al., 2005; Ziegler et al., 2011; Channell et al., 2009, 2018; Xuan et al., 2016). Absolute paleointensity data from lavas are hampered by unknown time gaps between lava flows and inadequate age control in young (Quaternary) lavas. RPI data from sediments have been acquired by normalizing the natural remanent magnetization (NRM) intensity by a laboratory-acquired magnetization designed to activate the same population of magnetic grains that carry the NRM, thereby compensating for variations in concentration of NRM-carrying grains throughout the sedimentary section. The laboratory-applied normalizers are typically anhysteretic remanent magnetization (ARM) and/or isothermal remanent magnetization (IRM). ARM is acquired in a decreasing alternating field (AF, with a peak AF of ~100 mT) with a weak direct current (DC) bias field (typically 50 μT), and IRM is acquired in a strong DC field (up to ~1 T). The appropriate normalizer is usually chosen such that its coercivity (response to AF demagnetization) closely matches that of the

NRM. A typical RPI proxy comprises the slope of NRM intensity versus ARM (and/or IRM) intensity determined over a particular peak demagnetization field range (such as 20-80 mT). The definition of the slope, often determined at 1-cm spacing down-core, can be gauged by determining its linear correlation coefficient (e.g., Xuan & Channell, 2009).

There is substantial agreement among late Quaternary stacks of global sedimentary RPI data (Valet et al., 2005; Channell et al., 2009; Ziegler et al., 2011; Xuan et al., 2016) that are independently supported by $^{10}Be/^{9}Be$ data from marine sediments (e.g., Simon et al., 2016) due to the role of the geomagnetic field in modulating cosmogenic isotope (^{10}Be) production. Agreement is, however, poor among stacks of sedimentary RPI data and $^{10}Be/^{9}Be$ data in the 0-40 ka interval (see Fig. 1 of Channell et al., 2018) that is attributed to subtle and often unrecognized drilling disturbance in poorly consolidated uppermost sediments recovered from the ocean floor. A recently published RPI stack for 10-40 ka based on high-deposition-rate sediments from the Iberian Margin and elsewhere (Fig. 1) is supported by paleointensity estimates from revised calculation of ^{10}Be flux in Greenland ice cores (Channell et al., 2018) using the GICC05 Greenland ice-core age model (Svensson et al., 2008). Models and stacks covering the same 0-40 ka interval that use RPI data from lower sedimentation rate sequences (e.g., Panovska et al., 2018) cannot resolve the detail that is revealed by higher sedimentation rate sequences and by ^{10}Be flux in ice cores.

When adequately recorded, "magnetic excursions" are manifested in both lavas and sediments as antipodal magnetization directions defining short-lived polarity reversal, and they occupy minima in RPI records (Laj & Channell, 2015). At least five magnetic excursions have been documented in lavas and sediments of the last 300 kyr (Fig. 1) with ~13 in the Brunhes Chron (last 775 kyr). Directional magnetic excursions have been named after the location where they were initially recorded such as Mono Lake (34 ka), Laschamp (41 ka), Blake (94 ka and 120 ka), Iceland Basin (191 ka) and Pringle Falls (211 and/or 238 ka). Although the first record of a magnetic excursion (the Laschamp excursion) was published over 50 years ago (Bonhommet & Babkine, 1967), magnetic excursions remain controversial mainly because the aberrant magnetization directions that define them have sub-millennial to millennial duration and are, therefore, fortuitously recorded in geological archives. Although the Laschamp excursion has now been recorded in scores of globally distributed sedimentary sequences (e.g., Laj et al., 2000, 2006; Mazaud et al., 2002; Lund et al., 2005; Evans et al., 2007; Collins et al., 2012; Channell et al., 2017), the Laschamp records represent a tiny proportion of the total number of paleomagnetically-studied sedimentary sequences that cover the Laschamp interval. The sub-millennial duration of the excursion means that recordings of the excursion are generally restricted to sequences with mean sedimentation rates >10-15 cm/kyr that are unusual in deep-sea sediments (see Roberts & Winklehofer, 2004). Lava records of the Laschamp are restricted to the Massif Central in France (e.g., Laj et al., 2014), the Auckland volcanic field (Cassata et al., 2008) and New Zealand's Mt. Ruapehu (Ingham et al., 2017), that just happened to have erupted with high frequency during this brief period.

The age of the Laschamp excursion, and the low geomagnetic field strength associated with it (Fig. 1), is based on correlation of deep-sea cores that record the Laschamp excursion to ice-core chronologies (e.g., Laj et al., 2000; Nowaczyk et al., 2012; Channell

et al., 2017), by $^{40}Ar/^{39}Ar$ age determinations in lavas from the Massif Central (e.g., Laj et al., 2014), by U/Th ages in a speleothem from Missouri (Lascu et al., 2016), and by the age of the related cosmogenic-isotope flux peak in ice cores (Yiou et al., 1997; Baumgartner et al., 1998; Wagner et al., 2000; Svensson et al., 2006, 2008; Traversi et al., 2016). Current estimates of the duration and mid-point age of the Laschamp directional excursion are <1 kyr and 41 ka, respectively. A less abrupt geomagnetic field intensity decrease (over several kyr) defines a paleointensity minimum that brackets the directional excursion.

Directional records of the Iceland Basin excursion at ~190 ka have been recovered from numerous deep-sea sediment cores from the Northern Hemisphere (see review in Channell, 2014), in cores from Lake Baikal (Oda et al., 2002), and two sites from the South Atlantic ocean (Stoner et al., 2003; Channell et al., 2017). The age of the excursion has been established by correlation to marine oxygen isotope records, and to ice core records. There are no records of the Iceland Basin excursion from well-dated lava sequences.

Apart from the Laschamp and Iceland Basin excursions, magnetic excursions during the last 300 kyr are controversial because of the paucity of records and/or poor age control in available records. On the other hand, RPI records and hence recordings of RPI minima associated with the excursions are numerous, presumably because RPI minima associated with excursions are manifest over longer timescales than the associated directional excursions.

The Mono Lake excursion at ~34 ka has been recorded in both deep-sea sediments and lava flows (Channell, 2006; Cassata et al., 2008; Kissel et al., 2011, Laj et al. 2014; Negrini et al., 2014) as well as at Mono Lake in California (e.g., Benson et al., 2003), although the age at the Mono Lake type-location is controversial (e.g., Kent et al., 2002; Cassata et al., 2010). The age of a RPI minimum associated with the Mono Lake excursion can be estimated from a cosmogenic-isotope flux maximum in Greenland ice cores (Wagner et al., 2000; Muscheler et al., 2005).

Although the older of the two Blake excursions (94 and 120 ka) was first recorded almost 60 years ago (Smith & Foster, 1969), there have only been a handful of observations of either Blake excursion since (see Laj & Channell, 2015). The older Blake excursion has, however, been observed in diverse media: marine sediments (e.g., Tric et al., 1991), Chinese loess (e.g., Zhu et al., 1994) and a speleothem from Spain (Osete et al., 2012). The younger "Blake" excursion, also known as the Skalamaelifell excursion, has been observed in Icelandic lavas (Jicha et al., 2011). The age of the Pringle Falls excursion (at 211 ka and/or 238 ka) is not yet settled due to a lack of records in well-dated sequences (Herrero-Bervera et al., 1994; Singer et al., 2008; Singer, 2014; Laj & Channell, 2015).

An apparent RPI minimum at ~13 ka appears in some individual RPI records, as a notch in RPI stacks (Fig. 1), and in virtual axial dipole moment (VADM) proxies from ^{10}Be flux in Greenland ice cores (Channell et al., 2018). In one core from the Iberian Margin (MD01-2444), a pronounced RPI minimum at ~13 ka is associated with a directional magnetic excursion (Channell et al., 2013). The apparent RPI minimum at ~13 ka in core MD01-2444 coincides with the old-end of the 0-14 ka Holocene paleointensity

model of Pavón-Carrasco et al. (2014). The RPI stack of Channell et al. (2018) contains a prominent field intensity peak (VADM ~13 x 10^{22} Am^2) around 18-17 ka followed by a field collapse between 16 and 14 ka culminating in a minimum VADM value (~7 x 10^{22} Am^2) that has been smoothed by stacking (Fig. 1). The VADM decrease at 17-13 ka corresponds to a rate of decrease (12.1 nT/yr) that is comparable to the rate (12.7 nT/yr) observed in the ^{10}Be-derived field at the same time (Channell et al., 2018), and to the rates observed during the Laschamp/Mono Lake excursions (Laj & Kissel, 2015).

To provide a reference template for geomagnetic field intensity over the last ~300 kyr, we combine the RPI stack for 14-45 ka (Channell et al., 2018) with the Holocene model for 0-14 ka (Pavón-Carrasco et al., 2014) and with the PISO paleointensity stack (Channell et al., 2009) beyond 45 ka. This paleointensity template was calibrated to VADM by aligning it with Holocene archaeomagnetic models (Korte et al., 2011; Pavón-Carrasco et al., 2014; Constable et al., 2016) and assuming a value of ~1.5 x10^{22} Am^2 for the VADM minimum at the Laschamp excursion (Laj et al., 2014). This VADM template provides a proxy for geomagnetic intensity variations that is compared with events in mammalian evolution, in order to test potential linkages between geomagnetic field intensity variations and late Quaternary mammalian evolution.

3. Late Quaternary Extinctions (LQE)

Causes of extinction of mammalian megafauna (adult weight >45 kg) during the Late Quaternary, the so-called Late Quaternary Extinction (LQE), have been the subject of prolonged debate (e.g., Martin, 1967; Koch & Barnosky 2006; Stuart 2015). Prior to ~13 ka, the mammal assemblage of the Americas included large-bodied animals such as mammoth, horses, camels, saber-tooth cats, and the short-faced bear. Extinction was total for mammals larger than 1000 kg, >50% for size classes between 32 and 1000 kg, and ~20% for those between 10 and 32 kg (Koch & Barnosky, 2006). Within a short time window, >150 species were lost in the Americas, including all mammals over ~600 kg. An analogous catastrophic size-controlled LQE affected 14 of 16 Australian mammalian genera; however, extinction ages are at least ~30 kyr older than in North America. Although fewer species were affected by the LQE in Africa and Eurasia, a similar size-biased extinction has been observed with end-Pleistocene (~13 ka) ages being prominent. Current explanations for the LQE in North America and Australia involve a combination of two hypotheses: climate change, and "overkill" by human hunting, modulated by the knock-on effect of herbivore extinction on the environment and on the survivability of other groups (e.g., Owen-Smith, 1987). Although "overkill" was originally used to explain North American extinctions (Martin, 1967), a forerunner of the hypothesis was popular in 19th century Europe, before it was eventually abandoned as archaeological evidence for human migration showed little evidence for the impact of human hunting on the LQE. Grayson & Metzler (2003) argued that island settings (e.g., New Zealand or the West Indies), where human hunting and habitat degradation can be unequivocally associated with extinction, should not be the model for continental extinctions. Extraterrestrial impact as a contributing cause for the LQE in North America, and for the onset of the Younger Dryas cold period (Firestone et al., 2007), have not been supported by subsequent analyses (Pinter et al., 2011; Holliday et al., 2014).

In North America, the brief (~200 yr) duration of Clovis-tool finds at ~13 ka (e.g.,

Waters & Stafford, 2007) is usually associated with rapid dispersal of modern humans across North America, and is closely contemporaneous with the LQE peak. On the other hand, the lack of mammalian kill sites in the Clovis record argues against a direct linkage between Clovis technology and "overkill". Humans were present in North America at least several kyr prior to the Clovis horizon (Gilbert et al., 2008; Waters et al., 2011), and perhaps prior to ~24 ka (Bourgeon et al., 2017).

According to Faith & Surovell (2009), the LQE in North America was abrupt and requires a mechanism capable of wiping out ~35 genera across the continent in a "geological instant" in the 13.8-11.4 ka interval (Fig. 2), with the spread in last appearances being largely explained by an incomplete fossil record and the resulting Signor-Lipps effect (Signor & Lipps, 1982). Abrupt versus staggered megafaunal extinction at the LQE is central to determination of cause. In their "continental simulation", Faith & Surovell (2009) determined the empirical probability (3.4 %) of observing a terminal Pleistocene (10-12 ka) age from 1955 stratigraphic occurrences (from 31 genera) of which 66 taxa (from 16 genera) yield terminal Pleistocene ages, assuming that all occurrences are equally likely to receive a terminal Pleistocene age. The simulation randomly assigned pre- or post- 12 ka ages to all 1955 observations based on this probability (3.4 %). The total number of genera that received a terminal Pleistocene age was tallied for each of 10,000 simulations to determine the probability of observing 16 or fewer terminal Pleistocene genera. The authors concluded that the observed pattern is consistent with synchronous (i.e., 10-12 ka) extinction for all 31 genera.

Bradshaw et al. (2012) proposed a Gaussian-resampled, inverse-weighted McInerny (GRIWM) approach, which weights observations inversely according to their temporal distance from the last observation of a confirmed species occurrence, and samples radiometric ages from the underlying probability distribution. In Figure 2, we show GRIWM estimates of continent-wide European extinctions from the fossil record aided by DNA analyses (Cooper et al., 2015), excluding regional disappearances. An extinction age estimate in North America for *Arctodus simus* (the short-faced bear) at 10.8 ka (Schubert, 2010) and the onset of population decline of *Bison priscus* (the steppe bison) at ~37 ka (Shapiro et al., 2004) are included in Figure 2. Note that the horse and woolly mammoth (*Mammuthus primigenius*) persisted in interior Alaska until ~10.5 ka (Haile et al., 2009), and the woolly mammoth survived on St. Paul Island (Alaska) until ~5.6 ka (Graham et al., 2016). Zazula et al. (2014) pointed out that the American mastodon (*Mammut americanum*) occupied eastern Beringia (Alaska/Yukon) during the last interglacial before its range contracted southward at the onset of glacial conditions at ~75 ka. The range of the species appears to have expanded northward again as interglacial conditions returned at the end of the Pleistocene, before extinction of the species at ~11.5 ka (10,000 ^{14}C years BP). Zazula et al. (2014) posed the question: why was this species stopped in its tracks when favorable conditions beckoned in Beringia?

An important proxy for herbivore population is the abundance in sedimentary sequences of coprophilous (dung) fungal spores, such as *Sporormiella*. The proxy was first proposed over 30 years ago (Davis, 1987), requires careful interpretation and laboratory techniques (e.g., van Asperen et al., 2016), but provides a measure of herbivore population independent of the bone-fossil record. Lake sediments in New York and Indiana imply a decline in *Sporormiella* spores beginning at 14.8 ka (Fig. 2)

that falls below the 2% threshold by 13.7 ka (Gill et al., 2009). This result has been closely replicated at Silver Lake (Ohio) where *Sporormiella* decline was dated at 13.9 ka (Gill et al., 2012). Importantly, the *Sporormiella* decline at these sites predates Younger Dryas cooling, and concurrent changes in the pollen record, and immediately predates a marked charcoal deposition increase, implying that herbivore decline and resulting landscape changes provide an explanation for subsequent (natural) landscape burning. The onset of the demise of North American herbivores at ~14.5 ka (Gill et al., 2009) lies within the Bølling-Allerød warm period with the Younger Dryas cold period beginning ~2 kyr later (e.g., Deplazes et al., 2013).

The South American LQE was even more profound than that in North America (Koch & Barnosky, 2006; Barnosky & Lindsey, 2010), with the loss of 50 megafaunal genera (~83%). Robust dates are scarce for the South American LQE, although it is appears that many taxa were lost near the Pleistocene-Holocene boundary (Barnosky & Lindsey, 2010). *Sporormiella* decline in lake sediments from SE Brazil imply herbivore population collapse at ~12 ka (Raczka et al., 2018).

In Northern Eurasia, 9 genera (35%) were lost during the LQE. Available age data are consistent with a two-phase extinction in the 45-35 ka and 15-10 ka intervals (Koch & Barnosky, 2006). Up to 50% of worldwide megafaunal extinctions at 15-10 ka apparently occurred in Northern Eurasia (Cooper et al., 2015), but the extinction pattern is more complex than in North America with megafaunal range contractions culminating in extinction for some species but not others (Stuart, 2015). In Figure 2, we plot continent-wide Eurasian megafaunal extinction events from Cooper et al. (2015). Several well-studied species disappeared continent-wide at ~26-31 ka (Fig. 2) hence their last appearances significantly postdate the Laschamp excursion (at ~41 ka). Post-Laschamp extinction for *Crocuta crocuta* (spotted hyaena) and *Crocuta spelaea* (cave hyaena) at ~26 ka were, however, preceded by severe range contraction from Asia into Europe (Stuart & Lister, 2014). Fossils of *Ursus spelaeus* (cave bear) also indicate E to W range contraction before extinction at ~26 ka with abrupt population decline, based on DNA analyses, after 50 ka (Stiller et al., 2010; Stiller et al., 2014; Baca et al., 2016).

In Africa, at least 24 species and ~10 genera of mammals became extinct in the 13-6 ka interval, representing 25% of Pleistocene African megafauna (Faith, 2014). Species-level extinction was, again, most intense for larger-bodied megafauna (Koch & Barnosky, 2006). The African LQE was considered to have been less severe than elsewhere, accounting for the relatively rich diversity of modern African megafauna. On the other hand, the number of extinct African species dated to the last 100 kyr exceeds the number in Europe and matches the number in Australia, and is only surpassed by the LQE in the Americas (Faith, 2014). In east Africa alone, the number of securely dated latest Pleistocene mammal extinctions has risen from two to seven in the last decade, with most being of grazers associated with open habitats (Faith, 2014).

Estimation of extinction ages for Australian megafauna (and for some Eurasian genera) is complicated by the majority of last appearances being at or beyond the practical range of radiocarbon dating (i.e., >40 ka). The LQE in Australia was apparently catastrophic for large mammalian megafauna, with the complete loss of all animals heavier than ~100 kg. Fourteen of sixteen genera of Pleistocene mammalian megafauna disappeared, together with all megafaunal reptiles (6 genera), in the vicinity of, or prior

434 to, ~40 ka (Fig. 2). Ten Australian genera disappeared in the 44-35 ka interval based on
435 a variety of frequentist statistical methods (including GRIWM) to determine extinction
436 ages for 16 megafaunal genera (Fig. 2; Saltré et al., 2016). The mass extinction of
437 megafauna at this time, including the largest-known (~3000 kg) marsupial
438 (*Diprotodon*), has been linked with climate variability and aridity (e.g., Wroe et al.,
439 2013) although this linkage has been disputed (e.g., Saltré et al. 2016), often in favor of
440 human predation or "overkill" (e.g., Brook & Johnson, 2006; Miller et al., 2016; Johnson
441 et al., 2016; van der Kaars et al., 2017). It is noteworthy that the extinction age for the
442 ~200-kg flightless bird *Genyornis newtoni* at ~35 ka (Fig. 2; Saltré et al., 2016) is
443 younger than the ~43 ka estimate given by Miller et al. (2016) based on dated eggshell
444 fragments. Even if final extinction was delayed until ~35 ka, the population of *Genyornis*
445 *newtoni* crashed close to the time of the Laschamp excursion (~41 ka) based on the egg-
446 shell data (Miller et al., 2016), although egg-shells attributed to *Genyornis newtoni* may
447 be from other species (Grellet-Tinner et al., 2016).
448
449 At Lynch's Crater (NE Queensland), an abrupt decline in dung fungi including
450 *Sporormiella* (Figs. 2 and 3) implies abrupt demise of large Australian herbivores at 40-
451 44 ka (Johnson et al., 2015). An abrupt increase in charcoal lags *Sporormiella* decline by
452 ~100 years, and evidence for grasses and sclerophyll vegetation lags *Sporormiella*
453 decline by ~300-400 years (Rule et al., 2012; Johnson et al., 2015). The charcoal-rich
454 levels can be explained by natural lightning-induced biomass burning as a result of fuel
455 build-up triggered by herbivore extinction (Rule et al., 2012; Johnson et al., 2016). Off
456 the southern coast of Western Australia, marine core MD03-2614G records a sharp
457 decline in *Sporormiella* in the 45-43 ka interval, relative to values recorded back to 140
458 ka (Figs. 2 and 3; van der Kaars et al., 2017).
459
460 A role for humans in the extinction of large animals in Australia remains popular (e.g.,
461 Brook & Johnson, 2006; Turney et al., 2008; Miller et al., 2016; Johnson et al., 2016; van
462 der Kaars et al., 2017), although the arrival of humans in Australia (Sahul) may have
463 predated the LQE at ~40 ka by ~25 kyr (Clarkson et al., 2017) although the arrival date
464 is not unequivocal (O'Connell et al., 2018). There is no evidence for a spike in the human
465 population in Australia at the time of the most prominent extinction event at ~40 ka,
466 when the entire Australian human population may not have exceeded a few tens of
467 thousands (Williams, 2013). Tasmania had a land bridge to the Australian mainland
468 during the last glacial, becoming an island in the early Holocene. The extinction of
469 megafauna in Tasmania at ~40 ka does not correspond to climate or environmental
470 change, and has been associated with the late arrival of humans in the region (Turney et
471 al., 2008). More recent results place the Tasmanian extinction of *Protemnodon anak* and
472 other megafauna at ~41 ka, predating human arrival on the island at ~39 ka and hence
473 precluding human involvement in the extinctions (Cosgrove et al., 2010; Lima-Ribeiro &
474 Diniz-Filho, 2014). Extant smaller (more accessible) prey, particularly the common
475 wombat (*Vombatus ursinus*) and the red-necked wallaby (*Macropus rufogriseus*),
476 characterize the early archaeological kill-sites on the island (Cosgrove et al., 2010).
477
478 Apart from Australian extinctions concentrated close to the Laschamp excursion at ~40
479 ka, fossils from the King's Creek Catchment (SE Queensland) indicate additional
480 concentrations of megafaunal last appearances at ~83 ka, ~107 ka and ~122 ka (Price
481 et al., 2011; Wroe et al., 2013). The older two dates (107 ka and 122 ka) correspond to
482 magnetic field intensity minima associated with the Blake excursions (Fig. 1b).

4. Neanderthal extinction

The extinction of Neanderthal represents one of the great puzzles of human evolution. Neanderthal and anatomically modern humans (AMHs) cohabited Western Europe for ~2-5 kyr, prior to ~39 ka, supporting the contention that competition may have contributed to the demise of Neanderthal (Higham et al., 2014). Brief cold and dry conditions in Europe associated with Heinrich Stadial (HS) 4 were proposed as an additional likely stressor on Neanderthal (Sepulchre et al., 2007). Analyses of Campanian Ignimbrite (CI) cryptotephra from archaeological sites in Greece and elsewhere in Eastern Europe and Libya indicated that the CI eruption occurred early in a dry period associated with HS4, postdated the end of the Middle Paleolithic and the Mousterian tool industry, and hence postdated the demise of Neanderthal (Lowe et al., 2012). In Black Sea sediment cores, CI tephra overlie, and therefore postdate, the Laschamp excursion (Nowaczyk et al, 2012).

The extinction of Neanderthal and the demise of the Mousterian tool industry (Fig. 3) can be placed at 41,030–39,260 calibrated years before present (41-39 ka) with 95.4% probability (Higham et al., 2014). Cooper et al. (2015) estimated the extinction of Neanderthal at 41,227 calibrated years before present (BP) with a standard deviation of 219 years, and 39,528-41,013 calibrated years BP using the GRIWM method (Fig. 2). Mousterian ages outside this range have been recorded at several locations in southern Iberia including Gorham's Cave in Gibraltar (Finlayson et al., 2006; Tzedakis et al., 2007), but these ages should now be disregarded according to Higham et al. (2014). Recent findings cast doubt on the existence of Neanderthal after ~39 ka, and lead to a closer correspondence of the demise of Neanderthals with the Laschamp magnetic excursion and the associated brief interval of very low geomagnetic field intensity centered at ~41 ka (Laj et al., 2014). It is important to note that the IntCal13 radiocarbon calibration (Reimer et al., 2013) may be offset to older ages by ~1 kyr in the vicinity of the Laschamp excursion, relative to ice-core chronologies (Muscheler et al., 2014).

Valet & Valladas (2010) proposed that low magnetic field strength in the Laschamp/Mono Lake excursion interval (40-33 ka) was an important factor in Neanderthal demise. Why anatomically modern humans (AMHs) were not similarly affected has remained an open question considering that the two populations shared habitats for 2600-5400 years (Higham et al. 2014) or >5 kyr (Lowe et al., 2012). There is no evidence for differences in skin pigmentation between European AMHs and Neanderthals, and at least a fraction of Neanderthals apparently had the same pale skin and/or red hair observed in some modern humans (Lalueza-Fox et al., 2007). Natural skin pigmentation in humans mitigates the harmful effects of UVR but its advantage is offset by the importance of sunlight for vitamin D3 synthesis. The skin protection factor (SPF) of "red ochre" (hematitic iron oxides) is traditionally utilized by some African tribes (Rifkin et al., 2015) and has been used since at least the last interglacial (~120 ka) based on ochre coatings on strung beads and residues on storage shells from Africa (Hodgskiss & Wadley, 2017), SE Spain (Hoffmann et al., 2018) and Levantine Mousterian sites (Bar-Yosef Mayer et al., 2009). The mystery of AMH survival at the time of Neanderthal demise may have been resolved by the discovery of differences in amino acid substitution in an intracellular chemosensor (the aryl hydrocarbon receptor,

AhR) for AMHs and for Neanderthals and other primates (Hubbard et al., 2016).

5. The role of the aryl hydrocarbon receptor (AhR)

Defense mechanisms against UVR include the production of quenching agents and anti-oxidant enzymes that neutralize reactive oxygen species (ROS) produced by UVR. The ROS modulation is controlled by the AhR intracellular chemosensor that plays a key role in the evolutionary response to UVR. Experimental results indicate an adaptive response of mitochondria to varying ROS levels under a phenomenon called mitohormesis (Becker et al., 2016).

The primary role of AhR is to regulate the transcription of genes mediating responses to the biochemical and toxic effects of dioxins, polyaromatic hydrocarbons, and related compounds (Abel & Haarmann-Stemmann, 2010). AhR is expressed in all skin cells and can be generated by UVR through an endogenous ligand formed in situ from an amino acid called tryptophan (Esser et al. 2009). UVR and the more harmful UVB (wavelength 290-320 nm) is absorbed by free tryptophan in the cytosol of epidermal cells, and AhR plays a key role in translocating UVR stress response to the nucleus (Wei et al., 1999; Fritsche et al., 2007; Tigges et al., 2014). Exposure to UVR, particularly UVB, generates highly mutagenic DNA photoproducts. The process initiates apoptosis and involves damage to nuclear DNA accompanied by mitochondrial dysfunction (Frauenstein et al., 2013). There is a general consensus that the AhR of modern humans is implicated in DNA repair (Schreck et al., 2009; Dittmann et al., 2016), tumor suppression (Fan et al., 2010; Yu et al., 2017), epidermal barrier function (Noakes 2015), skin tanning response, and melanocyte homeostasis (Luecke et al., 2010; Jux et al., 2011). Phylogenetic analysis suggested that the ability of vertebrate AhR to sense xenobiotics was acquired at a late stage of evolution, implying that the driving force for evolutionary conservation of AhR lies not only in its role in xenobiotic metabolism but also in normal cell development (Hao & Whitelaw, 2013; Hahn et al., 2017).

Hubbard et al. (2016) showed that the AhR variant in modern humans contains Val381 residue in the ligand-binding domain, while the AhR of Neanderthals, and a Denisovan individual, as well as non-human primates and other vertebrates (rodents) encode the ancestral Ala381 variant. The Val381 variant is fixed in the genome of all modern humans as well as in the genome of the oldest (45 ka) AMH individual sequenced to date (Fu et al., 2014). Hubbard et al. (2016) suggested that the unique modification of AhR in AMHs led to significant competitive advantage over their Neanderthal neighbors, due to decreased sensitivity in AMHs to toxins associated with fire-smoke, the effects of which may have been exacerbated by troglodytic lifestyles.

Our focus here is on AhR involvement in the regulation of the skin responses to UVR, especially to harmful UVB radiation, and its modulation of the immune system (Rannug & Fritsche, 2006; Agostinis et al., 2007; Esser et al., 2013). UVB induces two signaling routes in mammalian cells: first, UVB is absorbed by nuclear DNA that results in generation of DNA photoproducts, and second, UVB activates cell-surface receptors (Merk et al., 2004). AhR plays an important role in skin integrity and immunity. AhR activation leads to transcriptional gene activation, and is involved in the cutaneous stress response to UVR (Agostinis et al., 2007; Dittmann et al., 2016; Schwarz, 2005; Navid et al., 2013) and alterations of gene expression (Dugo et al., 2012). Activation of

AhR by UVB leads to signaling both to the nucleus and to cell membranes (Fritsche et al., 2007). The findings show that UVB irradiation affects cell surface receptors with subsequent activation of mitogen-activated protein kinases that in turn affect DNA in the nucleus.

6. The early fossil record of *Homo sapiens*

From analyses of the fossil and stone-tool record over the last 250 kyr (Fig. 4), Lahr (2016) proposed five transitions in the evolutionary history of *Homo sapiens*. (1) The origins of the species at 240–200 ka; (2) the first major expansion at 130–100 ka; (3) a period of dispersals at 70–50 ka; (4) a period of local/regional structuring of diversity at 45–25 ka; and (5) an early Holocene phase of significant extinction of hunter–gatherers and expansion of farmers (the Holocene Filter).

Until recently, Member 1 of the (Omo) Kibish Formation of Ethiopia yielded the earliest known AMH cranial remains (Day et al., 1969). A volcanic tuff about 2 m below the level of the fossil finds has a $^{40}Ar/^{39}Ar$ weighted mean age of 196 ± 2 ka (McDougall et al., 2005). An age of 196 ka for Member 1, combined with sedimentological evidence for rapid deposition, are consistent with Member 1 having been deposited synchronously with Mediterranean sapropel S7 (McDougall et al., 2008, Brown et al. 2012). Jebel Irhoud, Morocco, has been an important archaeological site since the 1960s when human fossils were found alongside Mousterian stone tools and were once dated at ~40 ka (Ennouchi, 1962). Recent fossil discoveries at this location support the presence of fossils with characteristics of AMHs (Hublin et al., 2017), and new luminescence age dating (Richter et al., 2017) indicates that the fossils are considerably older, at ~300 ka, than the Ethiopian AMH finds at Omo Kibish (Fig. 4). The finds in Morocco are now among the earliest known hominin fossils with AMH characteristics, in common with characteristics of the Florisbad fossil from South Africa discovered by T.F. Dreyer in 1932 and dated at ~260 ka (Grün et al., 1996). With such a sparse hominin fossil record, it is not possible to predict when AMHs first appeared, although the period from 300 ka to 200 ka in Africa appears to have been a critical time in development of AMH, and may constitute the evolutionary cradle of our species.

7. Time to most recent common ancestor (TMRCA) from mtDNA and Y-chromosomes

Thirty years ago, Cann et al. (1987) demonstrated that ethnically diverse surveys of modern mitochondrial DNA (mtDNA) are a major source of human evolutionary history. The advantages of mtDNA as an evolutionary tool include faster mutation rates in mtDNA than in nuclear genes, and mtDNA is inherited maternally and does not recombine. Cann et al. (1987) demonstrated the African origin of the human mitochrondrial gene pool, and estimated that mtDNA stems from an African mitochrondrial "Eve" who lived approximately 200,000 years ago. Initially, this conclusion met with considerable resistance, however, increasing numbers of studies, including work on Y-chromosomes, imply that the "Eve" hypothesis is substantially correct. There is now broad consensus for the "out-of-Africa" hypothesis whereby modern humans appeared at ~200 ka in Africa and spread throughout the continent before dispersing across the globe, although the exact chronology and nature of the population divergence remains unclear (Zhou & Teo, 2016). Dispersal has resulted in

630 the occupation of a wide variety of habitats with selection in response to specific
631 ecological pressures. A complete understanding of adaptation depends on a description
632 of the genetic mechanisms and selective history that underlies heritable traits (e.g.,
633 Radwan & Babik, 2012), and the signatures of natural selection are a response to
634 selective pressures that are often unknown. Estimating the age of selection signals may
635 allow reconstruction of the history of environmental changes that shaped human
636 phenotypes with specific ages associated with human dispersal out-of-Africa and the
637 spread of agriculture (Nakagome et al., 2016).
638
639 Both mtDNA and Y-chromosomes have been used to reconstruct human history. The
640 former (mtDNA) is often the better option for analyzing ancient DNA because it is easier
641 to obtain, is present in higher number in human cells, and does not undergo
642 recombination. However, mtDNA reflects only the maternal history of a population and
643 the history of a single individual may not accurately reflect the history of a population.
644 For this reason, mtDNA studies should be complemented by data on the male-specific Y-
645 chromosome (Pakendorf & Stoneking, 2005). Rates of human evolution have been
646 estimated by applying a number of substitution models to mtDNA or Y-chromosome
647 sequence data (Behar et al., 2008; Soares et al., 2013; Wang et al., 2014; Kivisild, 2015).
648 In some examples, calibration has relied on the assumption that the genetic separation
649 between humans and chimpanzees occurred at ~6 Ma, and that the evolutionary
650 process has been clocklike since that time, while more complex models involve different
651 substitution rates for coding and control regions of the genome (see Endicott et al.,
652 2009). Molecular clocks can be tested by comparison with archaeological data
653 pertaining to human migration.
654
655 Phylogeny based on the first complete mtDNA sequence data available in
656 year 2000 (from 52 individuals selected from around the world) yielded a
657 time to the most recent common ancestor (TMRCA) of ~190 ka (see
658 Oppenheimer, 2003, 2009; Soares et al. 2009), apparently consistent with the
659 conclusions of Cann et al. (1987) and with dated fossil finds of early AMH in Ethiopia
660 (McDougall et al., 2005). More recent studies of human evolution from mtDNA
661 (Oppenheimer, 2012), and of paternal evolution from Y-chromosomes (Poznik et al.,
662 2016), yield a broadly consistent picture of human evolution over the last ~200 kyr
663 although the timing of branches in the evolutionary tree are poorly constrained and
664 depend on estimated rates of mutation and population size (Fig. 4). As pointed out by
665 Wang et al. (2014), Y-chromosomal substitution rates obtained using different
666 calibration modes vary considerably, and produce disparate reconstructions of human
667 history. An additional determinant of substitution rate is the efficacy of purifying
668 selection, which in turn depends not only on the particular constraints of each
669 chromosome, but also on the long-term effective population size for each chromosome
670 type (Elhaik et al., 2014). Furthermore, mutation rates may have changed during
671 hominoid evolution (Scally, 2016).
672
673 The TMRCA is not a unique number, but rather a probability distribution based on two
674 fundamental assumptions: the number of mutations and the mutation rate. Estimates of
675 TMRCA depend strongly on the substitution rate and different results can be obtained
676 by using different rates. For example, Mendez et al. (2013) estimated a very early date
677 of 338 ka for the TMRCA of the Y-chromosome tree (L00) from a population of African-
678 Americans. The authors explained this early age by either long-standing population

679 structure among modern human populations or archaic introgression from unknown
680 species into the ancestors of modern humans in western Central Africa. However, other
681 researchers (e.g., Wang et al., 2014) have pointed out that this ancient TMRCA can be
682 partially attributed to the low substitution rate used by the authors. By using either a
683 higher mutation rate or more extensive sequencing data, the estimate of TMRCA
684 becomes much younger at about 208 ka (Elhaik et al. 2014) or 257 ka (D'Atanasio et al.
685 2018).
686
687 Poznik et al. (2013) reported the entire Y-chromosome and mitochondrial genome
688 sequences using a within-human calibration point to estimate the substitution rate. The
689 results indicate small TMRCA differences from Y-chromosomes (120–156 ka) and
690 mtDNA (99-148 ka) that disagree with the conventional suggestion that the common
691 ancestor of male lineages lived considerably more recently than that of female lineages.
692 Analyzing the entire Y-chromosome dataset of the 1000 Genomes Project (2012, 2015),
693 using the pedigree-based substitution rate, Wang et al. (2014) estimated the TMRCA at
694 105 ka that is consistent with the estimate (105 ka) of Cruciani et al. (2011) and the
695 estimate (101-115 ka) of Wei et al. (2013).
696
697 Phylogeny based on mtDNA sequence data has provided an estimate of TMRCA (190 ka)
698 with branching episodes at ~120 ka, ~70 ka, ~40 ka and ~15 ka which coincide with
699 AMH dispersal patterns (Oppenheimer, 2012). Wei at al. (2013) used five substitution
700 models to assess phylogenetic nodes from the TMRCA of 29 Y-chromosomes that
701 yielded branching ages for one of the models (GENETREE-2) of 112 ±12 ka, 68 ±7 ka, 49
702 ±6 ka and 13 ±2 ka. Applying the BEAST method to 68 worldwide Y-chromosomes,
703 Scozzari et al. (2014) dated the first two splits in their tree at ~196 ka and ~167 ka,
704 followed by TMRCAs at ~110 ka, 85-77 ka, 51-33 ka and 8-22 ka (Fig. 4).
705
706 It remains challenging to reconstruct population structure prior to ~60 ka using
707 existing data, but the modern-human African mtDNA pool contains phylogenetic
708 patterns that can be used to estimate the ages of several haplogroups. Analyzing L0
709 HVS-I sequences, Rito et al. (2013) classified five branches (L0a, L0b, L0d, L0f, and L0k)
710 of the mtDNA tree. The age estimates indicate that the mtDNA tree split to form L0 at
711 ~180 ka, and later diversity follows a geographical distribution from southern Africa
712 northward. Around ~128 ka, two distinct AMH groups co-existed in Africa with a first
713 split around 119 ka (L0k) followed by major clades at 98.7 ka (L0f), 70.9 ka (L0b) and
714 42.4 ka (L0a). It is noteworthy that the splitting of the widespread and common L0a, the
715 diversification of L0k, and population increases of both haplogroups L0 and L3 can be
716 dated to ~40 ka (Fig. 4).
717
718 **8. Discussion**

719 Past episodes of low geomagnetic dipole field strength affect UVR levels arriving at the
720 Earth's surface because reduction in magnetospheric shielding results in lower
721 stratospheric ozone levels, and hence lowered UVR shielding (Wei et al., 2014). Solar
722 storms enhance nitrogen oxide production in the stratosphere that, in early 2004, led to
723 ozone reduction of more than 60% at high northern latitudes (Randall et al., 2005).
724 Similarly, atmospheric N_2O concentrations are enhanced during times of low
725 geomagnetic field strength when shielding from solar storms and GCRs is diminished.
726 Earth's surface naturally emits N_2O from the oceans and from soils, with emissions

727 having increased due to anthropogenic practices. N_2O emissions are enhanced during
728 interglacial and interstadial (warm) climate states, and increased by ~50% at the last
729 glacial termination (Schilt et al., 2013, 2014). Enhanced atmospheric N_2O
730 concentrations during the Bølling-Allerød warm period, which coincided with an
731 apparent geomagnetic field strength minimum at ~13 ka, would have elevated UVR
732 reaching the Earth's surface at this time. It is noteworthy that the drastic magnetic field
733 intensity decrease after the peak at 18 ka (Fig. 1) coincided with paleoclimatic changes
734 especially in the southern hemisphere (Boex et al., 2013; Moreno et al., 2015; Martinez-
735 Garcia et al., 2014). Evidence from Antarctic ice cores indicates sudden enhanced
736 tropospheric UVR that has been related to a Mount Tahahe eruption dated to 17.7 ka
737 (McConnell et al., 2017).
738
739 A selection process resulted Neanderthal disappearance at ~41 ka that apparently did
740 not affect AMHs. Previous hypotheses for Neanderthal disappearance, and expansion of
741 AMHs, include differences in subsistence strategies, language skills, and technical,
742 economic and social systems, and the ability to adapt to changing environments (e.g.,
743 Kochiyama et al., 2018). Response to environmental change such as UVR flux at Earth's
744 surface would have involved the AhR, a chemosensor that regulates immunity and
745 differs in AMHs versus Neanderthals and other primates (Hubbard et al., 2016). Ages
746 for the end of the Mousterian tool industry and Neanderthal demise (Higham et al.,
747 2014) are now tightly constrained to the Laschamp magnetic excursion (at 41 ka)
748 implying a role for high UVR levels during the Laschamp field intensity minimum (Fig.
749 3).
750
751 Prominent low geomagnetic field intensity episodes at 285 ka, 190 ka, 110-120 ka, 64
752 ka, 41 ka and 13 ka (Fig. 1) appear to correspond to important times in evolution of
753 hominins and other large mammals. At the LQE, megafauna in Australia, Europe and the
754 Americas were thought to have become extinct over a protracted time in the Late
755 Quaternary, however, improved age estimates and discovery of new fossil sites (Roberts
756 et al., 2001; Koch & Barnosky, 2006; Faith & Surovell, 2009; Barnosky & Lindsey, 2010;
757 Price et al., 2011; Wroe et al., 2013; Stuart, 2015; Faith, 2014; Cooper et al., 2015; Saltré
758 et al., 2016) have led to extinction peaks becoming progressively constrained to ~13 ka
759 in the Americas, to ~40 ka (with earlier episodes at 84, 107 and 122 ka) in Australia,
760 and a complex combination of late Pleistocene ages (including ~13 ka and ~40 ka) in
761 Eurasia and Africa.
762
763 One of the outstanding and intriguing aspects of the LQE is the strong correlation
764 between extinction and body mass. As the vast majority of cell mutations are
765 deleterious, large long-lived organisms are at an evolutionary disadvantage. In addition,
766 small mammals often have opportunities to avoid UVR through burrowing. In modern
767 mammal populations, there is, however, no apparent correlation between body mass
768 and cancer occurrence, known as Peto's Paradox (Peto et al., 1975). The elephant
769 genome includes 20 copies of an oncogene (TP53) that is a crucial tumor suppressor
770 gene involved in apoptosis in response to DNA damage, whereas other mammals
771 usually have small numbers of this gene (Abeggelen et al., 2015; Sulak et al., 2016). This
772 discovery may explain why elephants are one of few large mammals to pass the LQE
773 barrier. On the other hand, the remains of two extinct mammoth species included more
774 than a dozen copies of TP53 in their genomes, and the American mastodon, that
775 disappeared at ~ 50 ka, had 3-8 copies in its genome which implies an evolutionary

776 selective trend in the increased number of copies of TP53 in the genomes of these
777 related megafauna (Sulak et al., 2016). TP53 is considered the guardian of the genome
778 due to its role in mitigating DNA damage, and is itself a target of UV-induced mutations
779 (Aylon & Oren, 2011; de Pedro et al. 2018).
780
781 Huang et al. (2017) analyzed the body weight of species in two orders of large ungulate
782 herbivores (Artiodactyla and Perissodactyla) from the Neogene fossil record in Europe
783 and North America. They found a significant and progressive increase in body weight
784 from early Miocene to late Pliocene for both orders in North America and for
785 Artiodactyla in Europe. This work was followed by the analysis of Smith et al. (2018)
786 who documented a global increase in body-size of megafauna during the Cenozoic, with
787 abrupt downsizing at the LQE in late Pleistocene. We speculate that large mammals may
788 have reached a natural body-size limit by late Pleistocene, due to increased likelihood of
789 cell mutation at times of high UVR flux, as life spans and body weights increased during
790 the Cenozoic. The envisaged role of UVB in reducing megafaunal populations at the LQE
791 does not involve an instantaneous "blitzkrieg", but rather an accumulation of UVB-
792 triggered mutations over multiple (~30) generations or ~0.5-1 kyr, the approximate
793 duration of RPI minima associated with magnetic excursions.
794
795 There is no clear correlation of LQE events, either at ~13 ka (in North America and
796 Eurasia), or ~40 ka (in Australia and Eurasia), with the first appearances of humans,
797 which apparently preceded the LQE by at least 10 kyr in Australia, and at least several
798 kyr in North America. The human population of Australia at ~40 ka was likely no more
799 than a few tens of thousands, with no evidence of an increase in population at this time
800 (Williams, 2013). According to Webb (2013), the "overkill" hypothesis *"is more*
801 *sensational, granted, but the arguments are unrealistic and the evidence for it, at least in*
802 *Australia, is non-existent*". The case for "overkill" in North America at ~13 ka involves
803 the close coincidence of the LQE with the brief (few century duration) Clovis-tool
804 horizon. On the other hand, based on *Sporormiella* decline in lake sediments from the
805 eastern USA, the demise at North American herbivores began at ~14.5 ka (Gill et al.,
806 2009, 2012), prior to the first appearance of Clovis tools. Clovis tools have only rarely
807 been found in association with megafaunal remains. Evidence for pre-Clovis human
808 occupation in the Americas includes locations in southern Chile (Dillehay et al., 2015),
809 and the Florida panhandle where human occupation at ~14.5 ka predated the
810 *Sporormiella* decline by ~2 kyr (Halligan et al., 2016), consistent with *Sporormiella*
811 disappearance at ~12.7 ka at another Florida panhandle location (Perotti, 2018).
812 Paucity of evidence for human occupation prior to ~13 ka can be attributed to
813 habitation being concentrated in coastal regions that were largely submerged during
814 the subsequent (last) deglaciation, when sea-level rise necessitated migration of
815 humans and other terrestrial mammals into the continental interior. We speculate that
816 large mammals, particularly those that did not burrow, were particularly susceptible to
817 DNA damage associated with low geomagnetic field strength and the resulting increase
818 in UVB reaching the Earth's surface. The coincidence of low magnetic field strength with
819 LQE events, particularly at ~40 ka and ~13 ka, but also at 107 ka and 122 ka in
820 Australia, implies that UVB flux was a contributing cause of the LQE in North America,
821 Europe and Australia.
822
823 The ~190 ka paleointensity minimum at the Iceland Basin excursion corresponds to
824 TMRCAs determined from the mtDNA and Y-chromosomes of modern humans (Gonder

et al., 2007; Soares et al. 2009; Oppenheimer, 2009, 2012; Wei et al., 2013; Poznik et al., 2016). Other paleointensity minima at 110-120 ka, 64 ka, 41 ka and 13 ka (Fig. 1) correspond to branches in phylogeny estimated from mtDNA and Y-chromosome analyses (Fig. 4). For example, Wei et al. (2013) used five models to assess phylogenetic nodes from the TMRCA of 29 Y-chromosomes that yielded branching ages for one model (GENETREE-2) of 112 ±12 ka, 68 ±7 ka, 49 ±6 ka and 13 ±2 ka, corresponding closely to minima in relative paleointensity records (Figs. 1 and 4). Although the transition from Middle Paleolithic to Upper Paleolithic at ~40 ka did not correspond to significant changes in AMH anatomy in the fossil record, it is an important time for human population structure (Fig. 4; Lahr, 2016) with mtDNA implying rapid population growth at a time of major advance in tool design and the first appearance of artwork (Stoneking, 1994).

Phylogeography, the study of human dispersal, demonstrates that when migration occurs from one region to another, new mutations unique to that region accumulate (Soares et al. 2016). Local adaption to different habitats, including changes in exposure to mutagenic solar radiation, partially controlled by the magnetic field, are potential sources of phenotypical divergence (Jablonski & Chaplin, 2000, 2010). During migrations, humans have adapted to differences in climate, altitude, and resource availability. Migration to new environments alters selection pressures on the human genome, and genetic studies have identified certain loci that were likely targets of this selection. For example, highly pigmented skin protects against skin cancer but reduces synthesis of vitamin D3, so differences in the amount of UVR place differing selection pressures on pigmentation genes (Creanza & Feldman, 2016).

9. Conclusions and Outlook

Although coincidence does not prove causality, the timing of geomagnetic field strength minima (hence enhanced UVR flux at Earth's surface) appears to correspond to events in mammalian evolution. Improvements in knowledge of past geomagnetic field strength, new mammalian fossil finds, advances in radiocarbon dating and DNA analyses of fossils, use of dung-fungal proxies for herbivore populations, and advances in the use of mtDNA and Y-chromosomes to map human phylogeny, have all contributed to this possible linkage. Minima in geomagnetic dipole field strength at ~13 ka and ~41 ka (Laschamp, Fig. 1) led to stratospheric ozone depletion and UVB levels at the Earth's surface that may have contributed to extinction of large mammals at these times, although extinction dates are associated with large errors due to the inadequacy of the fossil record (Fig. 2). The Neanderthals were apparently victims of the ~41 ka (Laschamp) magnetic field minimum, and differences in the AhR of modern humans and Neanderthals may explain why we passed the Laschamp evolutionary barrier. Episodes of low field strength further back in time notably at ~64 ka, ~110-120 ka (Blake, Fig. 1), and ~190 ka (Iceland Basin, Fig. 1) may have contributed to phylogenetic nodes in hominin evolution revealed by fossil finds and by studies of mtDNA and Y-chromosomes (Fig. 4). According to this hypothesis, the geomagnetic field influenced evolution of large long-lived mammals through exposure to UVR at times of low field strength, with foci of the extinction (e.g. Australia and Europe at ~41 ka, and North America and Europe at ~13 ka) depending on the specific geometry of stratospheric ozone depletion during episodes of low field strength. Ozone holes are preferentially located at high latitudes because of the role of stratospheric temperatures and polar

stratospheric clouds (PSC) in ozone depletion. UVR arriving at the Earth's surface may have had an influence on evolution due its strong mutagenic effects, its potential for promoting oxidative damage on membranes and proteins, and the role of AhR in translocating UVB stress response to the nucleus. Lower levels of UVR reaching Earth's surface at low latitudes, due to the role of polar-stratospheric clouds and stratospheric temperature in ozone depletion, may partly explain the relative diversity of modern African megafauna.

As the chronologies of both the relative paleointensity record and the paleontological record become better resolved, we speculate that unconvincing efforts to establish a linkage between polarity reversal and extinction over the last ~50 years will, in future, be superseded by a linkage between extinction and paleointensity minima particularly for land-dwelling mammals at higher latitudes where the magnetic field strength is linked to loss of stratospheric ozone and enhanced UVR reaching Earth's surface. The importance of Australian extinction events at the time of Laschamp excursion (41 ka) and the Blake excursions (107 and 120 ka) may imply that stratospheric ozone depletion was largely in the Southern Hemisphere at these times, and in the Northern Hemisphere when the North American extinctions are manifested at ~13 ka.

The magnetic dipole moment has decreased by ~10% since 1833 (Gauss' first direct field intensity measurement), or ~5% per century. Although the present dipole field strength may not be appreciably lower than the average during the Brunhes Chron, the current field intensity decrease, combined with asymmetry in the field detected in satellite data, has led to speculations that the geomagnetic field may reach intensity levels appropriate for a magnetic excursion or polarity reversal in the next 1000-2000 years (Hulot et al., 2002; Glassmeier et al., 2009; Laj & Kissel, 2015).

Twenty years ago, no more than 5 Quaternary magnetic excursions had been recorded (see Opdyke & Channell, 1996), whereas today ~20 Quaternary magnetic excursions have credible documentation (Laj & Channell, 2015). In the next few decades, we speculate that integration of excursion records with RPI and cosmogenic isotope records, understanding of the role of the geomagnetic field in controlling UVR flux and the role of Ahr in modulating the deleterious effects of UVR in extant and fossil mammals, documentation of mammalian extinction, and improvements in human phylogeny from mtDNA and Y-chromosomes, will clarify the role of the geomagnetic field in mammalian evolution.

Acknowledgements: We are very grateful to Christopher Janus, Fulvio Cruciani, Andrew Roberts, three anonymous reviewers, and journal editor Fabio Florindo for comments that significantly improved the manuscript.

Figure Captions

Fig. 1. Relative paleointensity (RPI) calibrated to virtual axial dipole moment (VADM). (a) Overall RPI stack of 23 sedimentary records (red) with standard error (2σ) compared with the ^{10}Be-based VADM from Greenland ice cores (blue) filtered with cut-offs of 1/3000 yrs (dark blue) and 1/500 yrs (dashed light blue) (Channell et al., 2018). Also shown: Holocene VADM models of Constable et al. (2016) (green) and Pavón-Carrasco et al. (2014) (black). (b) PISO RPI stack for 40-300 ka (Channell et al., 2009). Yellow shading indicates RPI minima in the stack that have been associated with directional magnetic excursions. See text for references that document the labeled excursions.

Fig. 2. Geomagnetic field intensity (VADM) for the last 70 kyr compared with timing of continent-wide extinction events for genera from Australia (Saltré et al., 2016), Eurasia (Cooper et al., 2015), and North America (Faith & Surovell, 2009), including extinction of *Arctodus simus* (Schubert, 2010) and population decline for *Bison priscus* (Shapiro et al., 2004). Solid and dashed bars in the Eurasia record refer to fossil and DNA derived events, respectively. Last appearance datums (LADs) for extinct North American genera (Faith & Surovell, 2009) were recalibrated using Calib 7.1 (Stuiver et al., 2018) with 2σ errors for entries that pass selection criteria established by Meltzer & Mead (1985). Dung fungi (*Sporormiella* and *Podospora*) in sedimentary archives, proxies for herbivore population, are for North America (Gill et al., 2009) and Australia (Johnson et al., 2015; van der Kaars et al., 2017). Geomagnetic field intensity during the last 70 kyr (red) combines VADM for the last 14 kyr (Pavón-Carrasco et al., 2014), VADM for 14-45 ka (Channell et al., 2018), and the PISO VADM record (Channell et al., 2009) for 45-70 ka. The light blue band represents the VADM estimate from ^{36}Cl-flux in Greenland ice-cores (Muscheler et al., 2005). Dark blue line corresponds to the ice-core ^{10}Be-derived VADM record (Channell et al., 2018). Background shades of blue are scaled to the maximum (darker blue color) and minimum (white) VADM intensity in the 1.35-13.27 x 10^{22} Am^2 range.

Fig. 3. Geomagnetic field intensity (VADM) for the 35-50 ka interval compared to probability density functions for the timing of Neanderthal disappearance at different sites (blue) and for the end of the Mousterian tool industry (black) (Higham et al., 2014), with dung-fungal proxies for large herbivore extinctions from NE Queensland (green, Johnson et al., 2015) and southern Western Australia (open circles joined by purple line, van der Kaars et al., 2017). The yellow band represents the GLOPIS paleointensity record converted to VADM (Laj et al., 2004, 2014), the purple curve is the sedimentary VADM record with 2σ errors, and the red line is the VADM reconstructed from ^{10}Be flux in Greenland ice-cores (Channell et al., 2018). The gray shading indicates the age range associated with Neanderthal demise, and the temporal overlap between the two human groups (Neanderthals and Cro Magnon). The end of the Mousterian flint-tool industry has been dated at 39.260-41.030 ka (Higham et al., 2014), and 39.528-41.013 ka (Cooper et al., 2015), corresponding closely with low field intensity associated with the Laschamp geomagnetic excursion (39.7-41.9 ka) (Laj et al., 2014).

Fig. 4. (a) Schematic evolutionary history of *Homo sapiens* modified after Lahr (2016). The fossil record includes key fossil specimens from Eliye Springs, Guomde, Florisbad, Herto, Omo Kibish and hominins from Jebel Irhoud dated by Richter et al., (2017).

Black/gray lines represent modern humans, dark blue lines the Denisovans, and the light blue lines the Neanderthals. Neanderthal extinction has been drawn according to the timing of the end of the Mousterian tool industry at ~40 ka (Higham et al., 2014). (b) Estimates of the time to the most recent common ancestor (TMRCA) and phylogenetic nodes, from Y-chromosomes (blue icons) and mitochondrial DNA (mtDNA) (pink icons), according to different authors. For Scozzari et al. (2014), haplogroup B corresponds to the split between chromosomes found only in central-west Africa and chromosomes spread over sub-Saharan Africa whereas the node at 115 ka marks the separation between African specific and all remaining haplogroups. Data from Wei et al. (2013) (GENETREE-2 model) include the TMRCA of haplogroup A3 and three phylogenetic nodes considered by the authors of particular interest: DR (expansion of Y-chromosomes following the out-of-Africa migration), FR (paleolithic male lineage expansion), and R1b (Neolithic modern European chromosomes). The data from Rito et al. (2013) refer to different nodes of the typical African haplogroup L0. (c) Geomagnetic VADM for the last 300 kyr (red band) as in Figure 2, using the PISO VADM record (Channell et al., 2009) to extend the record back to 300 ka. The light blue band and the dark blue line represent the VADM estimate (from ^{36}Cl- and ^{10}Be-derived, respectively) from ice-cores as in Figure 2. The yellow line represents the VADM determined from the GLOPIS paleointensity stack from marine sediments (Laj et al., 2004, 2014). Magnetic excursions corresponding to paleointensity minima are labeled (see Fig. 1). Background shades of blue are scaled to the maximum (darker blue color) and minimum (white) VADM intensity in the 1.35-14.73 x 10^{22} Am^2 range.

990 **REFERENCES**
991
992 1000 Genomes Project Consortium, Abecasis, G. R., Auton, A., Brooks, L. D., De Pristo, M.
993 A., Durbin, R. M., Handsaker, R. E., et al. (2012). An integrated map of genetic variation
994 from 1,092 human genomes. *Nature*, **491**, 56-65.
995
996 1000 Genomes Project Consortium. (2015). A global reference for human genetic
997 variation. *Nature,* **526**, 68–74.
998
999 Abegglen, L. M., Caulin, A. F., Chan, A., Lee, K., Robinson, R., Campbell M. S., et al. (2015).
1000 Potential mechanisms for cancer resistance in elephants and comparative cellular
1001 response to DNA damage in humans. *Journal of the American Medical Association*
1002 *(JAMA),* **314** (17), 1850–1860.
1003
1004 Abel, J., & Haarmann-Stemmann, T. (2010). An introduction to the molecular basics of
1005 aryl hydrocarbon receptor biology. *Biological Chemistry,* **391**(11), 1235-48.
1006
1007 Agostinis, P., Garmyn, M., & Van Laethem, A. (2007). The Aryl hydrocarbon receptor: an
1008 illuminating effector of the UVB response. *Science's STKE.* **403**, pe49.
1009
1010 Aubry, M.-P., Van Couvering, J. A., Christie-Blick, N., Landing, E., Pratt, B. R., Owen, D. E.,
1011 & Ferrusquia-Villafranca, I. (2009). Terminology of geologic time: Eastablishment of a
1012 community standard. *Stratigraphy,* **6** (2), 100-105.
1013
1014 Aylon, Y. & Oren, M. (2011). p53: guardian of ploidy. *Molecular Oncology*, **5**, 315-323.
1015
1016 Baca, M., Popović, D., Stefaniak, D., Marciszak, A., Urbanowski, M., Nadachowski, A., &
1017 Mackiewicz, P. (2016). Retreat and extinction of the Late Pleistocene cave bear (*Ursus*
1018 *spelaeus* sensu lato). *The Science of Nature,* **103**, 92, 1-17.
1019
1020 Barnosky, A.D., & Lindsey, E.L. (2010). Timing of Quaternary megafaunal extinction in
1021 South America in relation to human arrival and climate change. *Quaternary*
1022 *International*, **217**, 10-29.
1023
1024 Bar-Yosef Mayer, D. E., Vandermeersch, B., & Bar-Yosef, O. (2009). Shells and ochre in
1025 Middle Paleolithic Qafzeh Cave, Israel: indications for modern behavior. *Journal of*
1026 *Human Evolution,* **56**, 307-314.
1027
1028 Baumgartner, S., Beer, J., Masarik, J., Wagner, G., Meynadier, L., & Synal, H.-A. (1998).
1029 Geomagnetic modulation of the ^{36}Cl flux in the GRIP ice core, Greenland. *Science*, **279**,
1030 1330–1332.
1031
1032 Bazhenov, M. L., Levashova, N. M., Meert, J. G., Golovanova, I. V., Danukalov, K. N., &
1033 Fedorova, N. M. (2016). Late Ediacaran magnetostratigraphy of Baltica: Evidence for
1034 Magnetic Field Hyperactivity? *Earth and Planetary Science Letters,* **435**, 124-135.
1035
1036 Behar, D. M., Villems, R., Soodyall, H., Blue-Smith, J., Pereira, L., Metspalu, E., et al. (2008).
1037 The Genographic Consortium. The dawn of human matrilineal diversity. *American*
1038 *Journal of Human Genetics*, **82**, 1130–1140.

Becker, A., Klapczynski, A., Kuch, N., Arpino, F., Simon-Keller, K., De La Torre, C., et al. (2016). Gene expression profiling reveals aryl hydrocarbon receptor as a possible target for photobiomodulation when using blue light. *Scientific Reports,* **6**, 33847; doi: 10.1038/srep33847.

Belisheva, N. K., Lammer, H., Biernat, H. K., & Vashenuyk, E. V. (2012). The effect of cosmic rays on biological systems: An investigation during GLE events, *Astrophysics and Space Sciences Transactions,* **8**, 7–17.

Benjamin, C. L., & Ananthaswamy, H. N. (2006). p53 and the pathogenesis of skin cancer. *Toxicology and Applied Pharmacology*, **224**, (3), 241-8.

Benson, L., Liddicoat, J., Smoot, J., Sarna-Wojcicki, A., Negrini, R., & Lund, S. (2003). Age of the Mono Lake excursion and associated tephra. *Quaternary Science Reviews*, **22**, 135–140.

Biggin, A. J., Piispa, E. J., Pesonen, L. J., Holme, R., Peterson, G. A., Veikkolainen, T., & Tauxe, L. (2015). Palaeomagnetic field intensity variations suggest Mesoproterozoic inner-core nucleation. *Nature,* **526**, 245-248.

Boex, J., Fogwill, C., Harrison, S., Glasser, N. F., Hein A., Schnabel, C., Xu, S. (2013). Rapid thinning of the late Pleistocene Patagonian Ice Sheet followed migration of the Southern Westerlies. *Scientific Reports*, **3**, 2118. doi: 10.1038/srep02118.

Bonhommet, N., & Babkine, J. (1967). Sur la présence d'aimantations inversées dans la Chaîne des Puys. *Comptes Rendus de l'Académie des Sciences Paris*, **264**, 92-94.

Bourgeon, L., Burke, A., & Higham, T. (2017). Earliest human presence in North America dated to the last glacial maximum: new radiocarbon dates from bluefish caves, Canada. *PLOS ONE,* **12**(1), e0169486.

Bradshaw, C. J. A., Cooper, A., Turney, C. S. M., & Brook, B. W. (2012). Robust estimates of extinction time in the geological record. *Quaternary Science Reviews*, **33**, 14-19.

Branze, D., & Foiani, M. (2008). Regulation of DNA repair throughout the cell cycle. *Nature Reviews Molecular Cell Biology*, **9**, 297–308.

Brook, B.W. & Johnson, C.N. (2006). Selective hunting of juveniles as a cause of the imperceptible overkill of the Australian Pleistocene megafauna. *Alcheringa*, **30**, 39-48.

Brown, F. H., McDougall, I., & Fleagle, J. G. (2012). Correlation of the KHS Tuff of the Kibish Formation to volcanic ash layers at other sites, and the age of early Homo sapiens (Omo I and Omo II). *Journal of Human Evolution*, **63**, 4, 577-585.

Canfield, D. E., Poulton, S. W., & Narbonne, G. M. (2007). Late-Neoproterozoic deep-ocean oxygenation and the rise of animal life. *Science*, **315**, 92-95.

1085 Cann, R. L. Stoneking, M., & Wilson, A. C. (1987). Mitochondrial DNA and human
1086 evolution. *Nature,* **325**, 31–36.
1087
1088 Cassata, W. S., Singer, B. S., & Cassidy, J. (2008), Laschamp and Mono Lake excursions
1089 recorded in New Zealand. *Earth and Planetary Science Letters,* **268**, 76–88.
1090 doi:10.1016/j.epsl.2008.01.009.
1091
1092 Cassata, W. S., Singer, B. S., Liddicoat, J. C., & Coe, R. S. (2010) Reconciling discrepant
1093 chronologies for the geomagnetic excursion in the Mono Basin, California: Insights from
1094 new $^{40}Ar/^{39}Ar$ dating experiments and a revised relative paleointensity correlation.
1095 *Quaternary Geochronology*, **5**, 533-543.
1096
1097 Channell, J. E. T. (2006). Late Brunhes polarity excursions (Mono Lake, Laschamp,
1098 Iceland Basin and Pringle Falls) recorded at ODP Site 919 (Irminger Basin). *Earth and*
1099 *Planetary Science Letters,* **244**, 378-393.
1100
1101 Channell, J. E. T., Xuan, C., & Hodell, D. A. (2009). Stacking paleointensity and oxygen
1102 isotope data for the last 1.5 Myr (PISO-1500). *Earth and Planetary Science Letters,* **283**,
1103 14–23.
1104
1105 Channell, J. E. T., Hodell, D. A., Margaric, V., Skinner, L. C., Tzedakis, P. C., & Kesler, M. S.
1106 (2013). Biogenic magnetite, detrital hematite, and relative paleointensity in Quaternary
1107 sediments from the Southwest Iberian Margin. *Earth and Planetary Science Letters,* **376**,
1108 99-109.
1109
1110 Channell, J. E. T. (2014), The Iceland Basin excursion: Age duration, and excursion field
1111 geometry, *Geochemistry Geophysics Geosystems*, **15**, 4920–4935,
1112 doi:10.1002/2014GC005564
1113
1114 Channell, J. E. T., Vázquez Riveiros, N., Gottschalk, J., Waelbroeck, C., & Skinner, L. C.
1115 (2017). Age and duration of Laschamp and Iceland Basin geomagnetic excursions in the
1116 South Atlantic Ocean. *Quaternary Science Reviews*, **167**, 1-13.
1117
1118 Channell, J. E. T., Hodell, D. A., Crowhurst, S. J., Skinner, L. C., & Muscheler, R. (2018).
1119 Relative paleointensity (RPI) in the latest Pleistocene (10-45 ka) and implications for
1120 deglacial atmospheric radiocarbon. *Quaternary Science Reviews*, **191**, 57-72.
1121
1122 Clancy, S. (2008). DNA damage and repair: mechanisms for maintaining DNA integrity.
1123 *Nature Education*, **1** (1), 103.
1124
1125 Clarkson, C., Jacobs, Z., Marwick, B., Fullagar, R., Wallis, L., Smith, M., et al. (2017).
1126 Human occupation of Australia by 65,000 years. *Nature,* **547** (7663), 306–310.
1127
1128 Collins, L. G., Hounslow, M. W., Allen, C. S., Hodgson, D. A., Pike, J., & Karloukovski, V. V.
1129 (2012). Palaeomagnetic and biostratigraphic dating of marine sediments from the
1130 Scotia Sea, Antarctica: first identification of the Laschamp excursion in the
1131 Southern Ocean. *Quaternary Geochronology,* **7**, 67-75.
1132

1133 Constable, C., Korte, M., & Panovska, S. (2016) Persistent high paleosecular variation
1134 activity in southern hemisphere for at least 10,000 years. *Earth and Planetary Science*
1135 *Letters*, **453**, 78-86.
1136
1137 Cooper, A., Turney, C., Hughen, K. A., Brook, B. W., McDonald, H. G., & Bradshaw, C. J. A.
1138 (2015). Abrupt warming events drove Late Pleistocene Holarctic megafaunal turnover.
1139 *Science,* **349**(6248), 602-606.
1140
1141 Cosgrove, R., Field, J., Garvey, J., Brenner-Coltrain, J., Goede, A., Charles, B. et al., (2010).
1142 Overdone overkill – the archaeological perspective on Tasmanian megafaunal
1143 extinctions. *Journal of Archaeological Science*, **37**, 2486-2503.
1144
1145 Creanza, N., & Feldman, M. W. (2014). Worldwide genetic and cultural change in human
1146 evolution. *Current Opinion in Genetics & Development*, **41**, 85-92,
1147 https://doi.org/10.1016/j.gde.2016.08.006.
1148
1149 Cruciani, F., Trombetta, B., Massaia, A., Destro-Bisol, G., Sellitto, D., & Scozzari, R. (2011).
1150 A revised root for the human Y chromosomal phylogenetic tree: The origin of patrilineal
1151 diversity in Africa. *American Journal of Human Genetics,* **88** (6), 814–818.
1152
1153 D'Atanasio, E., Trombetta, B., Bonito, M., Finocchio, A., De Vito, G., Seghizzi, M. et al.
1154 (2018). The peopling of the last green Sahara revealed by high-coverage resequencing
1155 of trans-Saharan patrilineages. *Genome Biology*, **19**: 20. doi.org/10.1186/s13059-018-
1156 1393-5
1157
1158 Day, M. H. (1969). Omo human skeletal remains. *Nature*, **222**, 1135-1138.
1159
1160 Davis, O. K., (1987). Spores of the dung fungus *Sporormiella*: increased abundance in
1161 historic sediments and before Pleistocene megafaunal extinction. *Quaternary Research,*
1162 **28**, 290–294
1163
1164 Delp, M. D., Charvat, J. M., Limoli, C. L., Globus, R. K., & Ghosh, P. (2016). Apollo lunar
1165 astronauts show higher cardiovascular disease mortality: possible deep space radiation
1166 Effects on the Vascular Endothelium. *Scientific Reports*, **6**, 29901.
1167
1168 de Pedro, I., Alonso-Lecue, P., Sanz-Gomez, N., Freije, A., & Gandarillas, A. (2018).
1169 Sublethal UV irradiation induces squamous differentiation via a p53-independent, DNA
1170 damage-mitosis checkpoint. *Cell Death & Disease*, **9**(11): 1094. doi.10.1038/s4149-018-
1171 1130-8
1172
1173 Deplazes, G., Lückge, A., Peterson, L. C., Timmermann, A., Hamann, Y., Hughen K. A., et al.
1174 (2013). Links between tropical rainfall and North Atlantic climate during the last glacial
1175 period, *Nature Geoscience,* **6**, 213-217.
1176
1177 Dillehay, T. D., Ocampo, C., Saavedra, J., Sawakuchi, A. O., Vega, R. M., Pino, M., et al.
1178 (2015). New archaeological evidence for an early human presence at Monte Verde,
1179 Chile. *PLOS ONE,* **10**(11), e0141923.
1180

1181 Dittmann, K. H., Rothmund, M. C., Paasch, A., Mayer, C., Fehrenbacher, B., Schaller, M., et
1182 al. (2016). The nuclear aryl hydocarbon receptor is involved in regulation of DNA repair
1183 and cell survival following treatment with ionizing radiation. *Toxicology Letters,* **240**(1),
1184 122-9.
1185
1186 Doglioni, C., Pignatti, J., & Coleman, M. (2016). Why did life develop on the surface of the
1187 Earth in the Cambrian? *Geoscience Frontiers **7**,* 6*,* 865-873.
1188
1189 Dugo, M. A., Han, F., & Tchounwou, P. B. (2012). Persistent polar depletion of
1190 stratospheric ozone and emergent mechanisms of ultraviolet radiation-mediated health
1191 dysregulation. *Reviews on Environmental Health,* **27**, 103–116.
1192
1193 Elhaik, E., Tatarinova, T., Klyosov, A., & Graur, D. (2014). The "extremely ancient"
1194 chromosome that isn't: A forensic bioinformatics investigation of Albert Perry's X-
1195 degenerate portion of the Y chromosome. *European Journal of Human Genetics*, **22**,
1196 1111–1116. doi: 10.1038/ejhg.2013.303
1197
1198 Endicott, P., Ho, S. Y. W., Metspalu, M., & Stringer, C. (2009). Evaluating the
1199 mitochondrial timescale of human evolution. *Trends in Ecology & Evolution, **24***, 515–
1200 521.
1201
1202 Ennouchi, E. (1962). Un Néanderthalien: l'homme du Jebel Irhoud (Maroc).
1203 *Anthropologie*, **66**, 279–299.
1204
1205 Esser, C., Rannug, A., & Stockinger, B. (2009). The aryl hydrocarbon receptor in
1206 immunity. *Trends in Immunology,* **30**, 447–454.
1207
1208 Esser, C., Bargen, I., Weighardt, H., Haarmann-Stemmann, T., & Krutmann, J. (2013).
1209 Functions of the Aryl Hydrocarbon Receptor in the skin. *Seminars in Immunopathology,*
1210 **35**(6), 677-691.
1211
1212 Evans, H. F., Channell, J. E. T., Stoner, J. S., Hillaire-Marcel, C., Wright, J. D., Neitzke, L. C., &
1213 Mountain, G. S. (2007). Paleointensity-assisted chronostratigraphy of detrital layers on
1214 the Eirik Drift (North Atlantic) since marine isotope stage 11, *Geochemistry Geophysics.*
1215 *Geosystems*, **8**, Q11007, doi:10.1029/2007GC001720
1216
1217 Faith, J. T. (2014). Late Pleistocene and Holocene mammal extinctions on continental
1218 Africa. *Earth Science Reviews*, **128**, 105-121.
1219
1220 Faith, J. T., & Surovell, T. A. (2009). Synchronous extinction of North America's
1221 Pleistocene mammals. *Proceedings of the National Academy of Sciences USA,* **106**, 20641-
1222 20645.
1223
1224 Fan, Y., Boivin, G. P., Knudsen, E. S., Nebert, D. W., Xia, Y., & Puga, A. (2010). The aryl
1225 hydrocarbon receptor functions as a tumor suppressor of liver carcinogenesis. *Cancer*
1226 *Research,* **70**, 212-20.
1227

1228 Finlayson, C., Giles Pacheco, F., Rodriguez-Vidal, J., Fa, A. D., Gutierrez López, J. M.,
1229 Santiago Pérez, A. et al. (2006). Late survival of Neanderthals at the southernmost
1230 extreme of Europe. *Nature,* **443**, 850-853.
1231
1232 Firestone, R. B., West, A., Kennett, J. P., Becker, L., Bunch, T. E., Revay, Z. S., et al. (2007).
1233 Evidence for an extraterrestrial impact 12900 years ago that contributed to the
1234 megafaunal extinctions and the Younger Dryas cooling. *Proceedings of the National*
1235 *Academy of Sciences USA,* **104**, 16016–16021 (2007).
1236
1237 Frauenstein, K., Sydlik, U., Tigges J., Majora, M., Wiek, C., Hanenberg, H., et al. (2013).
1238 Evidence for a novel anti-apoptotic pathway in human keratinocytes involving the aryl
1239 hydrocarbon receptor, E2F1, and checkpoint kinase 1. *Cell Death & Differentiation*, **20**.
1240 1425–1434. doi: 10.1038/cdd.2013.102
1241
1242 Fritsche, E., Schäfer, C., Calles, C., Bernsmann, T., Bernshausen, T., Wurm, M., et al.
1243 (2007). Lightening up the UV response by identification of the aryl hydrocarbon
1244 receptor as a cytoplasmatic target for ultraviolet B radiation. *Proceedings of the National*
1245 *Academy of Sciences USA,* **104**, 8851-8856.
1246
1247 Fu, Q., Li, H., Moorjani, P., Jay, F., Slepchenko, S. M., Bondarev, A. A., et al. (2014). Genome
1248 sequence of a 45,000-year-old modern human from western Siberia. *Nature,* **514**, 445–
1249 449.
1250
1251 Gilbert, M. T., Jenkins D. L., Götherstrom A., Naveran N., Sanchez J. J., Hofreiter M., et al.
1252 (2008). DNA from pre-Clovis human coprolites in Oregon, North America. *Science,* **320**,
1253 786–789.
1254
1255 Gill, J. L., Williams, G. W., Jackson, S. T., Lininger, K. B., & Robinson, G. S. (2009).
1256 Pleistocene megafaunal collapse, novel plant communities, and enhanced fire regimes in
1257 North America. *Science,* **326**, 1100-1103.
1258
1259 Gill, J. L., Williams, J. W., Jackson, S. T., Donnelly, J. P., & Schellinger, G. C. (2012). Climatic
1260 and megaherbivory controls on late-glacial vegetation dynamics: a new, high-resolution,
1261 multi-proxy record from Silver Lake, Ohio. *Quaternary Science Reviews*, **34**, 66-80.
1262
1263 Glassmeier, K. H., Richter, O., Vogt, J., Möbus, P. & Schwalb, A., (2009). The Sun,
1264 geomagnetic polarity transitions, and possible biospheric effects: review and
1265 illustrating model. *International Journal of Astrobiology*, **8**, 147–159.
1266 doi:10.1017/S1473550409990073
1267
1268 Glassmeier, K. H., & Vogt, J. (2010). Magnetic polarity transitions and biospheric effects.
1269 *Space Science Reviews,* **155** (1-4), 387-410.
1270
1271 Gonder, M. K., Mortensen, H. M., Reed, F. A., de Sousa, A., & Tishkoff, S. A. (2007). Whole-
1272 mtDNA genome sequence analysis of ancient African lineages. *Molecular Biology and*
1273 *Evolution*, **24**, 757-768.
1274
1275 Graham, R. W., Belmecheri, S., Choy, K., Culleton, B. J., Davies, L. J., Froese, D. et al.,
1276 (2016). Timing and causes of mid-Holocene mammoth extinction on St. Paul Island,

Alaska. *Proceedings of the National Academy of Sciences USA*, 113 (33), doi/10.1073/pnas.1604903113

Grayson, D. K., & Meltzler, D. J. (2003). A requiem for North American overkill. *Journal of Archaeological Science*, **30**, 585-593.

Grellet-Tinner, G., Spooner, N. A., & Worthy, T. H. (2016). Is the "Genyornis" egg of a mihirung or another extinct bird from the Australian dreamtime? *Quaternary Science Reviews*, **133**, 147-164.

Grün, R., Brink, J. S., Spooner, N. A., Taylor, L., Stringer, C. B., Franciscus, R. B., Murray, A. S. (1996). Direct dating of Florisbad hominid. *Nature,* **382**, 500–501.

Hahn, M. E., Karchner, S. I., & Merson, R. R. (2017). Diversity as opportunity: Insights from 600 Million Years of AHR Evolution. *Current Opinion in Toxicology,* **2**, 58-71.

Haile, J., Froese, D. G., MacPhee, R. D. E., Roberts, R. G., Arnold, L. J., Reyes, A. V. et al. (2009). Ancient DNA reveals late survival of mammoth and horse in interior Alaska. *Proceedings of the National Academy of Sciences USA*, **106** (52), doi/10.1073/pnas.0912510106

Halligan, J. J., Waters, M. R., Perrotti, A., Owens, I. J. Feinberg, J. M., Bourne, M. D., et al. (2016). Pre-Clovis occupation 14,550 years ago at the Page-Ladson site, Florida, and the peopling of the Americas. *Science Advances,* **2**(5), e1600375.

Hao, N., & Whitelaw, M. L. (2013). The emerging roles of AhR in physiology and immunity. *Biochemical. Pharmacology,* **86**, 561-570.

Hays, L. D. (1971). Faunal extinctions and reversals of the earth's magnetic field. *Bulletin of the Geological Society of America,* **82**, 2433-2447.

Hernandez Moresino, R. D., Goncalves R. J., Helbling E. W. (2011). Sublethal effects of ultraviolet radiation on crab larvae of *Cyrtograpsus altimanus*. *Journal of Experimental Marine Biology and Ecology*, **407**, 363–369.

Herrero-Bervera, E., Helsley, C. E., Sarna-Wojcicki, A. M., Lajoie, K. R., Meyer, C. E., McWilliams, M. O., et al. (1994). Age and correlation of a paleomagnetic episode in the western United States by $^{40}Ar/^{39}Ar$ dating and tephrochronology: the Jamaica, Blake, or a new polarity episode? *Journal of Geophysical Research*, **99**, 24,091-24,103.

Hessen, D. O. (2008). Solar radiation and evolution of life. In: E. Bjertness (Ed.), *Solar Radiation and Human Health* (p. 123-136). The Norwegian Academy of Science and Letters, Oslo.

Higham, T., Douka, K., Wood, R., Ramsey, C. B., Brock, F., Basell, L., et al. (2014). The timing and spatiotemporal patterning of Neanderthal disappearance. *Nature,* **512**, 306–309.

1325 Hodgskiss, T., & Wadley, L. (2017). How people used ochre at Rose Cottage Cave, South
1326 Africa: Sixty thousand years of evidence from the Middle Stone Age. *PLOS ONE,* **12**(4),
1327 e0176317.
1328
1329 Hodgson, D.A., Vyverman, W., Verleyen, E., Leavitt, P.R., Sabbe, K., Squier, A.H. & Keely,
1330 B.J., (2005). Late Pleistocene record of elevated UV radiation in an Antarctic lake. *Earth*
1331 *and Planetary Science Letters*, **236**, 765-772.
1332
1333 Hoffmann, D. L., Angelucci, D. E ., Villaverde, V., Zapata, J., & Zilhao, J. (2018). Symbolic
1334 use of marine shells and mineral pigments by Iberian Neanderthals 115,00 years ago.
1335 *Science Advances*, **4**, eaar5255.
1336
1337 Holliday, V. T., Surovell, T., Meltzer, D. J., Grayson, D. K., & Boslough, M. (2014). The
1338 Younger Dryas impact hypothesis: a cosmic catastrophe. *Journal of Quaternary Science*,
1339 **29**, 515–530.
1340
1341 Hollosy, F. (2002). Effects of ultraviolet radiation on plant cells. *Micron*, **33**, 179-197.
1342
1343 Huang, S., Eronen, J. T., Janis, C. M., Saarinen, J. J., Silvestro, D., & Fritz, S. A. (2017).
1344 Mammal body size evolution in North America and Europe over 20 Myr: Similar trends
1345 generated by different processes. *Proceedings of the Royal Society of London* B, **284**,
1346 20162361.
1347
1348 Hubbard, T. D., Murray, I. A., Bisson, W. H., Sullivan, A. P., Sebastian, A., Perry, G. H., et al.
1349 (2016). Divergent Ah receptor ligand selectivity during hominin evolution. *Molecular*
1350 *Biology and Evolution,* **33**, 2648–2658.
1351
1352 Hublin, J. J., Ben-Ncer, A., Bailey, S. E., Freidline, S. E., Neubauer, S., M., Skinner, M. M.,
1353 Bergmann I., et al*.* (2017). New fossils from Jebel Irhoud Morocco and the pan-African
1354 origin of *Homo sapiens*. *Nature,* **546**, 289–292.
1355
1356 Hulot, G., Eymin, C., Langlais, B., Mandea, M., & Olsen, N. (2002). Small-scale structure of
1357 the geodynamo inferred from Oersted and Magsat satellite data, *Nature*, **416**, 620–623,
1358 doi:10.1038/416620
1359
1360 Ingham, E., Turner, G.M., Conway, C.E., Heslop, D., Roberts, A.P., Leonard, G., Townsend,
1361 D., & Calvert, A. (2017). Volcanic records of the Laschamp geomagnetic excursion from
1362 Mt. Ruapehu, New Zealand. *Earth and Planetary Science Letters*, **472**, 131-141.
1363
1364 Jablonski, N. G., & Chaplin, G. (2000). The evolution of human skin coloration. *Journal of*
1365 *Human Evolution,* **39**, 57–106.
1366
1367 Jablonski, N. G., & Chaplin, G. (2010). Human skin pigmentation as an adaptation to UV
1368 radiation. *Proceedings of the National Academy of Sciences USA,* **107**, 8962–8968.
1369
1370 Jicha, B. R., Kristjánsson, L., Brown, M. C., Singer, B. S., Beard, B. L., & Johnson, C. M.
1371 (2011). New age for the Skálamælifell excursion and identification of a global
1372 geomagnetic event in the late Brunhes chron. *Earth and Planetary Science Letters,* **310**,
1373 509-517.

Johnson, C. N., Rule, S., Haberle, S. G. Turney, C. S. M. Kershaw, A. P., & Brook, W. B. (2015). Using dung fungi to interpret decline and extinction of megaherbivores: problems and solutions. *Quaternary Science Reviews*, **110**, 107-113.

Johnson, C. N., Alroy, J., Beeton, N. J., Bird, M. I., Brook, B. W., Cooper, A., et al. (2016). What caused extinction of the Pleistocene megafauna of Sahul? *Proceedings of the Royal Society B,* **283**(1824), 20152399.

Jux, B., Kadow, Luecke, S., Rannug, A., Krutmann, J., & Esser, C. (2011). The aryl hydrocarbon receptor mediates UVB radiation-induced skin tanning. *Journal of Investigative Dermatology,* **131**, 203-210.

Kent, D. V.. Hemming, S. R., & Turrin, B. D. (2002). Laschamp excursion at Mono Lake? *Earth and Planetary Science Letters***, 197**, 151-164

Kissel, C., Guillou, H., Laj, C., Carracedo, J. C., Nomade, S., Perez-Torrado, F., & Wandres, C. (2011). The Mono Lake excursion recorded in phonolitic lavas from Tenerife (Canary Islands): Paleomagnetic analyses and coupled K/Ar and Ar/Ar dating. *Physics of the Earth and Planetary Interiors,* **187**, 232–244.

Kivisild, T. (2015). Maternal ancestry and population history from whole mitochondrial genomes. *Investigative. Genetics,* **10**(6), 3.

Koch, P. L., & Barnosky, A. D. (2006). Late Quaternary extinctions: state of the debate. *Annual Review of Ecology, Evolution, and Systematics,* **37**, 215–250.

Kochiyama, T., Ogihara, N., Tanabe, H. C., Kondo, O., Amano, H., Hasegawa, K., et al. (2018). Reconstructing the Neanderthal brain using computational anatomy. *Scientific Reports*, **8**, 6296. doi:10.1038/s41598-018-24331-0

Korte, M., Constable, C., Donadini, F., & Holme, R. (2011). Reconstructing the Holocene geomagnetic field. *Earth and Planetary Science Letters,* **312**, 497–505.

Lalueza-Fox, C., Römpler, H., Caramelli, D., Stäubert, C., Catalano, G., Hughes, D., et al. (2007). A melanocortin 1 receptor allele suggests varying pigmentation among Neanderthals. *Science*, **318**, 1453-1455.

Lahr, M. (2016). The shaping of human diversity: filters, boundaries and transitions. *Philosophical Transactions of the Royal Society B,* **371**, 20150241.

Laj, C., & Channell, J. E. T. (2015). "Geomagnetic excursions". In G. Schubert & M. Kono (Eds). *Treatise in Geophysics*, (2nd Edition, Vol. 5, Geomagnetism, pp. 343–386). Amsterdam: Elsevier.

Laj, C., Kissel, C., Mazaud, A., Channell, J. E. T., & Beer, J. (2000). North Atlantic palaeointensity stack since 75 ka (NAPIS-75) and the duration of the Laschamp event. *Philosophical Transactions of the Royal Society A,* **358**, 1009–1025.

1423 Laj, C., Kissel, C., & Beer, J. (2004). High resolution global paleointensity stack since 75
1424 kyrs (GLOPIS-75) calibrated to absolute values. In J. E. T. Channell, D. V. K. Kent, W.
1425 Lowrie, J. G. Meert (Eds). *Timescales of the Geomagnetic Field, AGU Monograph Series*
1426 (Vol. 145, pp. 255–265). Washington, DC, AGU.
1427
1428 Laj C., Kissel C., and Roberts A.P. (2006) Geomagnetic field behavior during the Icelandic
1429 Basin and Laschamp geomagnetic excursions: A simple transitional field geometry?
1430 *Geochemistry Geophysics Geosyst*ems, **7**, Q03004 (doi :10,1029/2005GC001122).
1431
1432 Laj, C., Guillou, H., & Kissel, C. (2014). Dynamics of the earth magnetic field in the 10-75
1433 kyr period comprising the Laschamp and Mono Lake excursions: new results from the
1434 French Chaîne des Puys in a global perspective. *Earth and Planetary Science Letters,*
1435 **387**, 184–197.
1436
1437 Laj, C., & Kissel, C. (2015). An impending geomagnetic transition? Hints from the past
1438 *Frontiers of Earth Science,* **3**, 10.3389/feart.2015.00061
1439
1440 Lascu, I., Feinberg, J. M., Dorale, J. A., Cheng, H., & Edwards, R. L. (2016). Age of the
1441 laschamp excursion determined by U-Th dating of a speleothem geomagnetic record
1442 from North America. *Geology*, **44**, 139-142.
1443
1444 Lima-Ribeiro, M. S., & Diniz-Filho, J. A. F. (2014). Obstinate overkill in Tasmania? The
1445 closest gaps do not probabilistically support human involvement in megafaunal
1446 extinctions. *Earth Science Reviews*, **135**, 59-64.
1447
1448 Lowe, J., Barton, N., Blockley, S., Ramsey, C. B., Cullen, V. L., Davies, W., et al. (2012).
1449 Volcanic ash layers illuminate the resilience of Neanderthals and early modern humans
1450 to natural hazards. *Proceedings of the National Academy of Sciences USA, **109***(34),
1451 13532-13537.
1452
1453 Luecke, S., Backlund, M., Jux, B., Esser, C., Krutmann, J., & Rannug. A. (2010). The aryl
1454 hydrocarbon receptor (AHR), a novel regulator of human melanogenesis. *Pigment Cell &*
1455 *Melanoma Research,* **23** (6), 828-33.
1456
1457 Lund S.P., Schwartz M., Keigwin L., & Johnson T. (2005). Deep-sea sediment records of
1458 the Laschamp geomagnetic field excursion (~41,000 calendar years before present):
1459 *Journal of Geophysical Research*, **110**, B04101. doi:10.1029/2003JB002943.
1460
1461 MacDavid K., & Aebischer D. (2014). A Review of sunlight induced cellular
1462 DNA damage. *American Journal of Cancer Therapy and Pharmacology*, **2**(1), 48-55.
1463
1464 Martin, P. S. (1967). Prehistoric overkill. In P.S. Martin, H. E. Wright Jr. (Eds), *Pleistocene*
1465 *Extinctions: The search for a Cause (*p. 75–120). Yale University Press, New Haven.
1466
1467 Martínez-García, A., Sigman, D. M., Ren, H., Anderson, R. F., Straub, M., Hodell, D. A., et al.
1468 (2014). Iron fertilization of the Subantarctic ocean during the last ice age. *Science*, **343**,
1469 1347–1350.
1470
1471 Mazaud, A., Sicre, M. A., Ezat, U., Pichon, J. J., Duprat, J., Laj, C., et al. (2002). Geomagnetic-

assisted stratigraphy and sea-surface temperature changes in core MD94-103 (southern Indian Ocean): Possible implications for north-south climatic relationship around H4. *Earth and Planetary Science Letters*, **201**, 159–170. doi:10.1016/S0012-821X(02)00662-3.

McConnell, J. R., Burke, A., Dunbar, N. W., Köhler, P., Thomas, J. L., Arienzo, M. M., et al. (2017). Synchronous volcanic eruptions and abrupt climate change~ 17.7 ka plausibly linked by stratospheric ozone depletion. *Proceedings of the National Academy of Sciences USA,* **114**(38), 10035-10040

McDougall, I., Brown, F. H., & Fleagle, J. G. (2005). Stratigraphic placement and age of modern humans from Kibish, Ethiopia. *Nature,* **433**, 733-736.

McDougall, I., Brown, F. H., & Fleagle, J. G. (2008). Sapropels and the age of hominins Omo I and II, Kibish, Ethiopia. *Journal of Human Evolution,* **55**, 409-4.

Meert, J. G., Levashova, N. M., Bazhenov, M. L., & Landing, E. (2016). Rapid changes of magnetic field polarity in the Late Ediacaran: Linking the Cambrian evolutionary radiation and increased UV-B radiation. *Gondwana Research,* **34**, 149-157.

Meltzer D.J., & Mead J. I. (1985). Dating late Pleistocene extinctions: Theoretical issues, analytical bias, and substantive results. In J. I. Mead, D. J. Meltzer (Eds.), *Environments and Extinctions: Man in Late Glacial North America* (pp. 145–173). Orono, ME: Center for the Study of Early Man, University of Maine.

Mendez, F. L., Krahn, T., Schrack, B., Krahn, A. M., Veeramah, K. R., Woerner, A. E., et al. (2013). An African American paternal lineage adds an extremely ancient root to the human Y chromosome phylogenetic tree. *American Journal of Human Genetics,* **92**, 454–459.

Mendoza, B., & de La Peña, S. (2010). Solar activity and human health at middle and low geomagnetic latitudes in Central America. *Advances in Space Research,* **46**, 449-459.

Merk, H. F., Abel, J., Baron, J. M., & Krutmann, J. (2004). Molecular pathways in dermatotoxicology. *Toxicology and Applied Pharmacology,* **195** (3), 267-77.

Miller, G., Magee, J., Smith, M., Baynes, A., Lehman, S., Spooner, N., et al. (2016). Human predation contributed to the extinction of the Australian megafaunal bird *Genyornis newtoni* ~47 ka. *Nature Communications*, **7**, 10496 (2016).

Moreno, A., Svensson, A., Brooks, S. J., Connor, S., Engels, S., Fletcher, W., et al. (2015). and data contributors: A compilation of Western European terrestrial records 60–8 ka BP: towards an understanding of latitudinal climatic gradients. *Quaternary Science Reviews*, **106,** 167-185.

Muscheler, R., Beer, J., Kublik, P. V., & Synal, H. A. (2005). Geomagnetic field intensity during the last 60,000 years based on ^{10}Be and ^{36}Cl from the Summit ice cores and ^{14}C. *Quaternary Science Reviews*, **24**, 1849-1860.

1521 Muscheler, R., Adolphi, F., & Svensson, A. (2014). Challenges in ^{14}C dating towards the
1522 limit of the method inferred from anchoring a floating tree ring radiocarbon chronology
1523 to ice core records around the Laschamp geomagnetic field minimum. *Earth and*
1524 *Planetary Science Letters*, **394**, 209-215.
1525
1526 Nakagome, S., Alkorta-Aranburu, G., Amato, R., Howie, B., Peter, BM., Hudson, R. R., & Di
1527 Rienzo, A. (2016). Estimating the ages of selection signals from different epochs in
1528 human history. *Molecular Biology and Evoution,* **333**, 657–669.
1529
1530 Navid, F., Bruhs, A., Schuller, W., Fritsche, E., Krutmann, J., Schwarz, T., & Schwarz, A.
1531 (2013). The aryl hydrocarbon receptor is involved in UVR-induced immunosuppression.
1532 *Journal of Investigative Dermatology,* **133**, 2763-2770.
1533
1534 Negrini, R. M., McCuan D. T., Horton R. A., Lopez J. D., Cassata W. S., Channell J. E.T., et al.
1535 (2014), Nongeocentric axial dipole field behavior during the Mono Lake excursion.
1536 *Journal of Geophysical Research Solid Earth*, **119**, doi:10.1002/2013JB010846.
1537
1538 Noakes, R. (2015). The aryl hydrocarbon receptor: a review of its role in the physiology
1539 and pathology of the integument and its relationship to the tryptophan metabolism.
1540 *International Journal of Tryptophan Research,* **8**, 7-18.
1541
1542 Nowaczyk, N. R., Arz, H. W., Frank, U., Kind J., & Plessen, B., (2012). Dynamics of the
1543 Laschamp geomagnetic excursion from Black Sea sediments. *Earth and Planetary*
1544 *Science Letters*, **351-352**, 54-69.
1545
1546 O'Connell, J. F., Allen, J., Williams, M. A. J., Williams, A. N., Turney, C. S. M., Spooner, N. A.,
1547 Kamminga, J., Brown, G., & Cooper, A. (2018). When did *Homo Sapiens* first reach
1548 Southeast Asia and Sahul? *Proceedings of the National Academy of Sciences USA,* **115**
1549 (34), doi/10.1073/pnas.1808385115
1550
1551 Oda, H., Nakamura, K., Ikehara, K., Nakano, T., Nishimura, M., & Khlystov, O. (2002).
1552 Paleomagnetic record from Academician Ridge, Lake Baikal: A reversal excursion at the
1553 base of marine oxygen isotope stage 6. *Earth and Planetary Science Letters*, **202**(1), 117-
1554 132. doi: 10.1016/S0012-821X(02)00755-0.
1555
1556 Opdyke, N. D., & Channell, J. E. T. (1996). *Magnetic Stratigraphy*. International
1557 Geophysics Series, (Vol. 64), 346 pp., Academic Press, San Diego, CA.
1558
1559 Oppenheimer, S. (2003). Out of Eden: The Peopling of the World. Constable & Robinson,
1560 London, 440 pp.
1561
1562 Oppenheimer, S. (2009). The great arc of dispersal of modern humans: Africa to
1563 Australia. *Quaternary International,* **202**, 2–13.
1564
1565 Oppenheimer, S. (2012). Out-of-Africa, the peopling of continents and islands: tracing
1566 uniparental gene trees across the map. *Philosophical Transactions of the Royal Society B:*
1567 *Biological Sciences,* **367**, 770–784.
1568

1569 Osete, M-L., Martin-Chivelet, J., Rossi, C., Edwards, R. L., Egli, R., Munoz-Garcia, M. B. et al.
1570 (2012). The Blake geomagnetic excursion recorded in a radiometrically dated
1571 speleothem. *Earth and Planetary Science Letters*, **353-354**, 173-181.
1572
1573 Owen-Smith, N. (1987). Pleistocene extinctions: the pivotal role of megaherbivores.
1574 *Paleobiology,* **13**, 351–62.
1575
1576 Pakendorf, B., & Stoneking, M. (2005). Mitochondrial DNA and human evolution. *Annual*
1577 *Review of Genomics and Human Genetics,* **6**, 165-183.
1578
1579 Panovska, S., Constable, S. G., & Korte, M. (2018) Extending global continuous
1580 geomagnetic field reconstructions on timescales beyond human civilization.
1581 *Geochemistry Geophysics Geosystems*, **19**, doi.org/10.1029/2018GC007966
1582
1583 Pavlov, V., & Gallet, Y. (2001). Middle Cambrian high magnetic reversal frequency
1584 (Kulumbe River section, northwestern Siberia) and reversal behavior during the Early
1585 Palaeozoic. *Earth and Planetary Science Letters***, 185**, 173–183.
1586
1587 Pavón-Carrasco, F. J., Osete, M. L., Torta, M. J., & De Santis, A. (2014). A geomagnetic field
1588 model for the Holocene based on archaeomagnetic and lava flow data. *Earth and*
1589 *Planetary Science Letters***, 388**, 98-109.
1590
1591 Perrotti, A. G. (2018). Pollen and *Sporormiella* evidence for terminal Pleistocene
1592 vegetation change and megafaunal extinction at Page-Ladson, Florida. *Quaternary*
1593 *International*, **466**(b), 256–268. https://doi.org/10.1016/j.quaint.2017.10.015
1594
1595 Peto, R., Roe, F. J., Lee, P. N., Levy, L., & Clack, J. (1975). Cancer and ageing in mice and
1596 men. *British Journal of Cancer,* **32**, 411–426.
1597
1598 Pinter, N., Scott, A. C., Daulton, T. L., Podoll, A., Koeberl, C., Anderson, R. S., & Ishman, S. E.
1599 (2011). The Younger Dryas impact hypothesis: A requiem. *Earth Science Reviews*, **106**,
1600 247–264.
1601
1602 Poznik, G. D., Henn, B. M., Yee, M. C., Sliwerska, E., Euskirchen, G. M., Lin A. A., et al.
1603 (2013). Sequencing Y chromosomes resolves discrepancy in time to common ancestor
1604 of males versus females. *Science,* **341**, 562–565.
1605
1606 Poznik, G. D., Xue, Y., Mendez, F. L., Willems, T. F., Massaia, A., Wilson Sayres, M. A., et al.
1607 (2016). 1000 Genomes Project Consortium, Punctuated bursts in human male
1608 demography inferred from 1,244 worldwide Y-chromosome sequences. *Nature Genetics,*
1609 **48**, 593–599.
1610
1611 Price, G. J., Webb, G. E., Zhao, J., Feng Y., Murray, A. S., Cooke, B. N., Hochnull, S. A., &
1612 Sobbe, I.H. (2011). Dating megafaunal extinction on the Pleistocene Darling Downs,
1613 eastern Australia: the promise and pitfalls of dating as a test of extinction hypotheses.
1614 *Quaternary Science Reviews*, **30**, 899-914.
1615
1616 Raczka, M. F., Bush, M. B., & De Oliveira, P. E. (2018). The collapse of megafaunal
1617 populations in southeastern Brazil. *Quaternary Research*, **89**, 103-118.

Radwan, J., & Babik, W. (2012). The genomics of adaptation. *Proceedings of the Royal Society B: Biological Sciences*, **279** (1749), 5024–5028. doi: 10.1098/rspb.2012.2322.

Randall, C. E., Harvey, V. L., Manney, G. L., Orsolini, Y., Codrescu, M., Sioris, C., et al. (2005). Stratospheric effects of energetic particle precipitation in 2003–2004. *Geophysical Research Letters,* **32**, Issue 5, L05802.

Randall, C. E., Harvey, V. L., Singleton, C. S., Bailey, S. M., Bernath, P. F., Codrescu, M., et al. (2007). Energetic particle precipitation effects on the Southern Hemisphere stratosphere in 1992-2005, *Journal of Geophysical Research*, **112**, D08308, doi:10.1029/2006JD007696.

Rannug, A., & Fritsche, E. (2006). The aryl hydrocarbon receptor and light. *Biological Chemistry,* **387**(9), 1149-57.

Raup, D. M. (1985). Magnetic reversals and mass extinctions. *Nature,* **314**, 341-343.

Raup, D. M., & Sepkoski, J. J. (1986). Periodic extinction of families and genera. *Science,* **231**, 833–836.

Reimer, P. J., Bard, E., Bayliss, A., Beck, J. W., Blackwell, P. G., Bronk Ramsey, C., et al. (2013). IntCal13 and Marine13 Radiocarbon Age Calibration Curves 0–50,000 Years cal BP. *Radiocarbon*, **55**(4), 1869-1887.

Richter, D., Grün, R., Joannes-Boyau, R., Steele, T. E., Amani, F., Rué, M., et al. (2017). The age of the hominin fossils from Jebel Irhoud, Morocco and the origins of the Middle Stone Age. *Nature,* **546**, 293-296.

Rifkin, R. F., Dayet, L., Queffelec, A., Summers, B., Lategan, M., & d'Errico, F. (2015). Evaluating the photoprotective effects of ochre on human skin by *in vivo* SPF assessment: Implications for human evolution, adaptation and dispersal. *PLOS ONE,* **10**(9), e0136090.

Rito, T., Richards, M. B., Fernandes, V., Alshamali, F., Cerny, V., Pereira, L., & Soares, P. (2013). The first modern human dispersals across Africa. *PLOS ONE*, **8**(11), e80031.

Roberts, A. P., & Winklhofer, M., 2004. Why are geomagnetic excursions not always recorded in sediments? Constraints from post-depositional remanent magnetization lock-in modelling. *Earth and Planetary Science Letters*, **227**, 345-359.

Roberts, R. G., Flannery, T. F., Ayliffe, L. K., Yoshida, H., Olley, J. M., Prideaux, G. J., et al., (2001). New ages for the last Australian megafauna: Continent-wide extinction about 46,000 years ago. *Science*, **292** (5523), 1888-1892. DOI: 10.1126/science.1060264

Rule, S., Brook, B. W., Haberle, S. G., Turney, C. S. M., Kershaw, A. P., & Johnson, C. N. (2012). The aftermath of megafaunal extinction: Ecosystem transformation in Pleistocene Australia. *Science,* **23** (335), 6075, 1483-1486.

1667 Saikawa, Y., Hashimoto, K., Nakata, M., Yoshihara, M., Nagai, K., Ida, M. & Komiya, T.
1668 (2014). The red sweat of the hippopotamus. *Nature*, **249**, 363.
1669
1670 Saltré, F., Rodríguez-Rey, M., Brook, B. W., Johnson, C. N., Turney, C. S. M., Alroy J., et al.
1671 (2016). Climate change not to blame for late Quaternary megafauna extinctions in
1672 Australia. *Nature. Communications*, **7**, 10511.
1673
1674 Scally, A. 2016. The mutation rate in human evolution and demographic inference.
1675 *Current Opinion in Genetics & Development,* **41**, 36–43
1676
1677 Schilt, A., Baumgartner, M., Eicher, O., Chappellaz, J. Schwander, J., Fischer, H., & Stocker,
1678 T. F. (2013). The response of atmospheric nitrous oxide to climate variations during the
1679 last glacial period. *Geophysical Research Letters,* **40**, 1888-1893.
1680
1681 Schilt, A., Brook E.J, Bauska, T.K., Baggenstos, D., Fischer, H., Joos, F. et al. (2014).
1682 Isotopic constraints on marine and terrestrial N_2O emissions during the last
1683 deglaciation. *Nature*, **516**, 234–237.
1684
1685 Schreck, I., Chudziak, D., Schneider, S., Seidel, A., Platt, K. L., Oesch, F., & Weiss, C. (2009).
1686 Influence of aryl hydrocarbon- (Ah) receptor and genotoxins on DNA repair gene
1687 expression and cell survival of mouse hepatoma cells. *Toxicology,* **259**(3), 91-96.
1688
1689 Schubert, B.W. (2010). Late Quaternary chronology and extinction of North American
1690 giant short-faced bears (*Arctodus simus*). *Quaternary International,* **217**, 188–194.
1691
1692 Schwarz, T. (2005). Mechanisms of UV-induced immunosuppression. *The Keio Journal of*
1693 *Medicine*, **54**, 165–171.
1694
1695 Scozzari, R., Massaia, A., Trombetta, B., Bellusci, G., Myres, N. M., Novelletto, A., &
1696 Cruciani, F. (2014). An unbiased resource of novel SNP markers provides a new
1697 chronology for the human Y chromosome and reveals a deep phylogenetic structure in
1698 Africa. *Genome Research,* **24**, 535–544.
1699
1700 Sepulchre, P., Ramstein, G., Kageyama, M., Vanhaeren, M., Krinner, G., Sánchez-Goñi, M.-
1701 F., & d'Errico, F. (2007). H4 abrupt event and late Neanderthal presence in Iberia. *Earth*
1702 *and Planetary Science Letters,* **258**, 283–292.
1703
1704 Shapiro, B., Drummond, A. J., Rambaut, A., Wilson, M. C., Matheus, P. E., Sher, A. V., et al.
1705 (2004). Rise and fall of Beringian steppe bison. *Science*, **306**, 1561-1565.
1706
1707 Signor III, P. W. & Lipps, J. H. (1982). Sampling bias, gradual extinction patterns, and
1708 catastrophes in the fossil record. In: *Geological implications of impacts of large asteroids*
1709 *and comets on the Earth* (ed. L. T. Silver and P. H. Schultz), Geological Society of America
1710 Special Publication, 190, 291–296.
1711
1712 Simon, Q., Thouveny, N., Bourlès, D. L., Valet, J. P., Bassinot, F., & Ménabréaz, L., et al.
1713 (2016). Authigenic $^{10}Be/^{9}Be$ ratio signatures of the cosmogenic nuclide production
1714 linked to geomagnetic dipole moment variation since the Brunhes/Matuyama
1715 boundary. *Journal of Geophysical Research*, **121**, 7716-7741.

Singer, B. S. (2014). A Quaternary geomagnetic instability time scale. *Quaternary Geochron*ology, **21**, 29-52.

Singer, B. S., Jicha, B. R., Kirby, B. T., Geissman, J. W., & Herrero-Bervera, E. (2008). $^{40}Ar/^{39}Ar$ dating links Albuquerque Volcanoes to the Pringle falls excursion and the geomagnetic instability time scale. *Earth and Planetary Science Letters***, 267**, 584-595.

Smith, F. A., Elliott Smith, R. E., Lyons, S. K. & Payne, J. L. (2018). Body size downgrading of mammals over the late Quaternary. *Science*, **360**, 310–313.

Smith J. D., & Foster J. H. (1969) Geomagnetic reversal in the Brunhes normal polarity epoch. *Science*, **163**, 565–567.

Soares, P., Ermini, L., Thomson, N., Mormina, M., Rito, T., Röhl, A., et al. (2009). Correcting for purifying selection: an improved human mitochondrial molecular clock. *American Journal of Human Genetics*, **84**, 740–759.

Soares, P., Abrantes, D., Rito, T., Thomson, N., Radivojac, P., Li, B., et al. (2013). Evaluating purifying selection in the mitochondrial DNA of various mammalian species. *PLOS ONE,* **8**(3), e58993.

Soares, P., Trejaut, J. A., Rito, T., Cavadas, B., Hill, C., Khong Eng, K., et al. (2016). Resolving the ancestry of Austronesian-speaking populations. *Human Genetics,* **135**, 309-326.

Stiller, M., Baryshnikov, G., Bocherens, H., Grandal d'Anglade, A., Hilpert, B., Münzel, S. C., et al. (2010). Withering away—25,000 years of genetic decline preceded cave bear extinction. *Molecular Biology and Evolution***, 27**(5), 975–978. https://doi.org/10.1093/molbev/msq083

Stiller, M., Molak, M., Prost, S., Rabeder, G. Baryshnikov, G., Rosendahl, W., et al., (2014). Mitochondrial DNA diversity and evolution of the Pleistocene cave bear complex. *Quaternary International,* **339-340**, 224-231.

Stoneking, M. (1994). Mitochondrial DNA and human evolution. *Journal of Bioenergetics and Biomembranes*, **26**(3), 251-259.

Stoner, J. S., Channell, J. E. T., Hodell, D. A., & Charles, C. D. (2003). A 580 kyr paleomagnetic record from the sub-Antarctic South Atlantic (Ocean Drilling Program Site 1089). *Journal of Geophysical Research*, **108**, B5, 2244. doi:10.1029/2001JB001390

Stuart, A. J. (2015). Late Quaternary megafaunal extinctions on the continents: a short review. *Geological Journal,* **50**, 338–363.

Stuart, A. J, & Lister, A.M. (2014). New radiocarbon evidence on the extirpation of the spotted hyaena (*Crocuta crocuta* (Erxl.)) in northern Eurasia. *Quaternary Science Reviews,* **96**, 108-116.

Stuiver, M., Reimer, P. J., & Reimer, R. W. (2018). CALIB 7.1 [WWW program] at http://calib.org, accessed 2018-3-2.

Sulak, M., Fong, L., Mika, K., Chigurupati, C., Yon, L., Mongan N. P., et al. (2016). TP53 copy number expansion is associated with the evolution of increased body size and an enhanced DNA damage response in elephants. *eLife,* **5**, e11994.

Suter, I., Zech, R., Anet, J. G., & Peter, T. (2014). Impact of geomagnetic excursions on atmospheric chemistry and dynamics. *Climate of the Past,* **10**, 1183-1194.

Svensson, A., Andersen, K. K., Bigler, M., Clausen, H. B., Dahl-Jensen, D., Davies, S. M., et al. (2006). The Greenland ice core chronology 2005, 15–42 ka. Part 2: comparison to other records. *Quaternary Science Reviews,* **25**, 3258-3267.

Svensson, A., Andersen, K. K., Bigler, M., Clausen, H. B., Dahl-Jensen, D., Davies, S. M., et al. (2008). A 60,000 year Greenland stratigraphic ice core chronology. *Climate of the Past,* **4**, 47-58.

Tigges, J., Haarmann-Stemmann, T., Vogel, C. F. A., Grindel, A., Hübenthal, U., Brenden, H., et al. (2014). The new aryl hydrocarbon receptor antagonist E/Z-2-benzylindene-5,6-dimethoxy-3,3-dimethylindan-1-one protects against UVB-induced signal transduction *Journal of Investigative Dermatology*, **134**(2), 556-559.

Traversi, R., Becagli, S., Poluianov, S., Severi, M., Solanki, S. K., Usoskin, I. G., & Udisti, R. (2016). The Laschamp geomagnetic excursion featured in nitrate record from EPICA-Dome C ice core. *Scientific Reports,* **6**, 20235.

Tric, E., C. Laj, C., J-P. Valet, J-P., P. Tucholka, P. M. Paterne, M., & F. Guichard, F. (1991). The Blake geomagnetic event: transition geometry, dynamical characteristics and geomagnetic significance. *Earth and Planetary Science Letters*, **102**, 1-13.

Turney, S.M., Flannery, T.F., Roberts, R.G., Reid, C., Fifield, L.K., Higham, T.F.G. et al. (2008). Late-surviving megafauna in Tasmania, Australia, implicate human involvement in their extinction. *Proceedings of the National Academy of Sciences USA,* **105** (34), doi/10.1073/pnas.0801360105

Tzedakis, P. C., Hughen, K. A., Cacho, I., & Harvati, K. (2007). Placing late Neanderthals in a climatic context. *Nature,* **449**, 206–208.

Valet, J. P., Meynadier, L., & Guyodo, Y. (2005). Geomagnetic dipole strength and reversal rate over the past two million years. *Nature,* **435**, 802–805.

Valet, J. P., & Valladas, H. (2010). The Laschamp-Mono lake geomagnetic events and the extinction of Neanderthal: a causal link or a coincidence? *Quaternary Science Reviews*, **29**, 3887–3893.

1812 van Asperen, E. N., Kirby, J. R., & Hunt, C. O. (2016). The effect of preparation methods
1813 on dung fungal spores: Implications for recognition of megafaunal populations. *Review*
1814 *of Palaeobotany and Palynology*, **229**, 1-8.
1815
1816 van der Kaars, S., Miller, G. H., Turney, C. S. M., Cook, E. J., Nurnberg, D., Schonfeld, J.,
1817 Kershaw, A. P., & Lehman, S. J. (2017). Humans rather than climate the primary cause of
1818 Pleistocene megafaunal extinction in Australia. *Nature Communications*, **8**: 14142.
1819 doi:10.1038/ncomms14142
1820
1821 Wagner, G., Beer, J., Laj, C. Kissel, C., Mazarik, J., Muscheler, R., & Synal, H. A. (2000).
1822 Chlorine-36 evidence for the Mono Lake event in the Summit GRIP ice core. *Earth and*
1823 *Planetary Science Letters,* **181**, 1–6.
1824
1825 Wang C.-C., Gilbert M. T. P., Jin L., & Li H. (2014). Evaluating the Y chromosomal
1826 timescale in human demographic and lineage dating. *Investigative Genetics*, **5**, 12. doi:
1827 10.1186/2041-2223-5-12
1828
1829 Waters, M. R., & Stafford Jr. T. W. (2007). Redefining the age of Clovis: Implications for
1830 the peopling of the Americas. *Science,* **315**, 5815, 1122-1126.
1831
1832 Waters, M. R., Stafford Jr., T. W., McDonald, H. G., Gustafson, C., Rasmussen, M.,
1833 Cappellini, E., et al. (2011). Pre-Clovis mastodon hunting 13,800 years ago at the Manis
1834 site, Washington. *Science,* **334**, 351–353.
1835
1836 Webb. S. (2013). *Corridors to extinction and the Australian megafauna*, 308pp., Elsevier,
1837 Amsterdam.
1838
1839 Wei, W*.,* Ayub, Q., Chen, Y., McCarthy, S., Hou, Y., Carbone, I., et al*.* (2013). A calibrated
1840 human Y-chromosomal phylogeny based on resequencing. *Genome Research.* **23**, 388–
1841 395.
1842
1843 Wei, Y. D., Rannug, U., & Rannug, A. (1999). UV-induced CYP1A1 gene expression in
1844 human cells is mediated by tryptophan. *Chemico-Biological Interactions,* **118**, 127-140.
1845
1846 Wei, Y., Pu, Z., Zong, Q., Wan, W., Ren, Z., Fraenz, M., et al. (2014). Oxygen escape from
1847 the Earth during geomagnetic reversals: Implications to mass extinction. *Earth and*
1848 *Planetary Science Letters,* **394**, 94-98.
1849
1850 Williams, A.N. (2013). A new population curve for prehistoric Australia. *Proceedings of*
1851 *the Royal Society of London* B, **280**: 20130486, doi.org/10.1098/rspb.2013.0486
1852
1853 Winkler, H., Sinnhuber, M., Notholt, J., Kallenrode, M.-B., Steinhilber, F., Vogt, J. et al.
1854 (2008). Modeling impacts of geomagnetic field variations on middle atmospheric ozone
1855 responses to solar proton events on long timescales. *Journal of Geophysical Research***,**
1856 **113**, D02302.
1857
1858 Wroe, S., Field, J. H., Archer, M., Grayson, D. K., Price, G. J., Louys, J., et al. (2013). Climate
1859 change frames debate over the extinction of megafauna in the Sahul (Pleistocene

Australia-New Guinea). *Proceedings of the National Academy of Sciences USA*, **110** (22), doi/10.1073/pnas.1302698110

Xuan, C., & Channell, J. E. T. (2009). UPmag: MATLAB software for viewing and processing u channel or other pass-through paleomagnetic data. *Geochemistry Geophysics Geosystems*, **10**, 1–12. http://dx.doi.org/10.1029/2009GC002584

Xuan, C., Channell, J. E. T., & Hodell, D. A. (2016). Quaternary magnetic and oxygen isotope stratigraphy in diatom-rich sediments of the southern Gardar Drift (IODP Site U1304, North Atlantic). *Quaternary Science Reviews,* **142**, 74-89. 10.1016/j.quascirev.2016.04.010.

Xue, Y., Wang, Q., Long, Q., Ng, B. L., Swerdlow, H., Burton, J., et al. (2009). Human Y chromosome base-substitution mutation rate measured by direct sequencing in a deep-rooting pedigree. *Current Biology*, **19**(17), 1453–1457. doi: 10.1016/j.cub.2009.07.032.

Yiou, F., Raisbeck, G. M., Baumgartner, S., Beer, J., Hammer, C., Johnsen, S., et al. (1997). ^{10}Be in the Greenland Ice Core Project ice core at Summit, Greenland. *Journal of Geophysical Research*, **102,** 26783-26794.

Yu, J. S., Leng, P. F., Li, Y. F., Wang, Y. Q.,Wang, Y., An, R. H., & Qi, J. P. (2017). Aryl hydrocarbon receptor suppresses the prostate cancer LNCaP cell growth and invasion by promoting DNA damage response under oxidative stress. *DNA. Cell Biology,* **36**(11), 1010-1017.

Zazula, G. D., MacPhee, R. D., Metcalfe, J. Z., Reyes, A. V., Brock, F., Druckenmiller P. S., et al. (2014). American mastodon extirpation in the Arctic and Subarctic predates human colonization and terminal Pleistocene climate change. *Proceedings of the National Academy of Sciences USA*, (**111**), 18460–18465. doi: 10.1073/pnas.1416072111

Ziegler, L. B., Constable, C. G., Johnson, C. L., & Tauxe, L. (2011). PADM2M: a penalized maximum likelihood model of the 0–2 Ma palaeomagnetic axial dipole moment. *Geophysical Journal International,* **184**, 1069-1089.

Zhou, J. & Teo Y.-Y. (2016). Estimating time to the most recent common ancestor (TMRCA): comparison and application of eight methods. *European Journal of Human Genetics,* **24**, 1195-1201.

Zhu, R.X., Zhou, L.P., Laj, C., Mazaud, A., & Ding, D.L. (1994). The Blake geomagnetic polarity episode recorded in Chinese loess. *Geophysical Research Letters*, **21**, 697-700.

GLOSSARY

6-4 photoproducts (6-4 PPs): 6-4 pyrimidine-pyrimidone photoproducts (6-4 PPs) and cyclobutane pyrimidine dimers (CPDs, see below) are the common UVR products formed in the human skin during exposure to sunlight. Although the 6-4 PPs are not as prevalent as CPDs (in lesion formation), they are significantly more mutagenic.

Anhysteretic remanent magnetization (ARM): A laboratory-induced remanent magnetization imparted by a strong alternating magnetic field in the presence of a weak direct current bias field. The bias field usually has an intensity comparable to the geomagnetic field. ARM provides an indication of magnetic mineral concentrations, and the efficiency of ARM acquisition varies with magnetic grain size.

Apoptosis: A form of programmed cell death that occurs in multicellular organisms. It is a highly regulated and controlled process that confers advantages during an organism's lifecycle. Because apoptosis cannot be halted once initiated, it is a highly regulated process.

Artiodactyla: Order of even-toed ungulates, hoofed animals that bear their weight on two toes including hippopotamuses, camels, antelopes, sheep, giraffes and deer.

Aryl hydrocarbon receptor (AhR): a protein that regulates gene expression, cell physiology and organ homeostasis with a key role in skin integrity and immunity. Its functions are related to cell proliferation, adhesion and migration as well as to cell differentiation. It has a strong function in mediating the response to xenobiotic and toxins particularly Dioxins, and to UVR.

Brunhes Chron: The most recent time interval of the geomagnetic polarity timescale, characterized by a normal polarity of the geomagnetic field, that has existed since ~773 ka.

Campanian Ignimbrite (CI): The Campanian Ignimbrite (CI) eruption was located near Napoli (Italy) and was probably the largest volcanic eruption in the Mediterranean region during the last 200 kyr. CI ash was deposited on the Russian Plain, and throughout the Eastern Mediterranean and northern Africa. The event coincided with the onset of a cold climatic phase known as Heinrich Stadial 4 (HS4) approximately 40,000 years ago.

Chlorofluorocarbons (CFCs): an organic compound (commonly known as Freon) that contains carbon, chlorine, and fluorine, produced as a volatile derivative of methane and ethane. Many CFCs have been commonly used as refrigerants, propellants (in aerosol applications), and solvents. Although the concentration of CFCs in the atmosphere is very small, measured in parts per trillion, they do contribute significantly to the enhancement of the greenhouse effect. CFCs contribute significantly to ozone depletion in the upper atmosphere. The manufacture of such compounds has been phased out under the Montreal Protocol, and their use is being replaced by other products such as hydrofluorocarbons.

Clades: In taxonomy, a clade is defined as a group of organisms consisting of a single common ancestor and all descendants of that ancestor.

Clovis horizon: The short-lived Clovis horizon comprises distinctive stone tools marking early human occupation of North America at ~13 ka. The Clovis culture is a prehistoric Paleo-Indian culture, named after characteristic stone tools found in close association with Late Pleistocene fauna at Blackwater near Clovis, New Mexico, in the 1920s and 1930s. Most of the indigenous cultures of the Americas are considered to descend from the Clovis people.

Coercivity: The coercivity, also called magnetic coercivity, is a measure of the ability of a remanent magnetization to withstand an external demagnetizing magnetic field. For ferromagnetic materials (*sensu lato*), the coercivity (or coercive force) is the intensity of the applied magnetic field required to reduce the remanent magnetization of that material to zero after the magnetization of the sample has been driven to saturation in the opposite direction.

Thus, coercivity measures the resistance of a ferromagnetic material (*sensu lato*) to demagnetization by an external field.

Cosmogenic isotopes: Radioactive isotopes created in the upper atmosphere when galactic cosmic rays collide with atmospheric molecules at high speed. The production rate of these isotopes depends on the intensity of the cosmic radiation, which is related to the strength of the Earth magnetic field and solar activity. Therefore, records of cosmogenic isotope production are useful for understanding the relation between the Earth magnetic field, and variations in solar activity.

Cyclobutane pyrimidine dimers (CPDs): One of two major photoproducts generated by UV irradiation. CPDs are molecular lesions formed in the human skin during exposure to sunlight due to UV radiation and photochemical reactions.

Cytosol: It is the fluid inside living cells. Proteins, organelles, and other structures of the cells live in this water-based fluid.

Deoxyribosyl: A univalent radical derived from deoxyribose, a monosaccharide (simple sugar). It is derived from the sugar as indicated by its name: deoxy sugar. Deoxyribose is the five-carbon sugar molecule involved to form the phosphate backbone of DNA molecules. DNA, or deoxyribonucleic acid, is a polymer formed of several nucleic acids. Each nucleic acid is composed by a molecule of deoxyribose bound to a phosphate group and either a purine or a pyrimidine. As part of DNA, 2-deoxyribose derivatives have a significant role in biology. The DNA molecule, which is the main repository of genetic information in life, consists of a long chain of deoxyribose-containing units called nucleotides, linked via phosphate groups.

DNA photoproducts: Exposure to the ultraviolet component of sunlight causes DNA damage, which subsequently leads to mutations, cellular transformation, and cell death through the creation of different photoproducts. There are two important DNA photoproducts, namely cyclobutane pyrimidine dimers (CPDs) and pyrimidine-pyrimidone photoproducts (6-4 PPs).

Endogenous ligand: A ligand is a protein that attaches (binds) to another protein called a receptor; the latter have specific sites into which the ligands fit like keys into locks. Ligands that are produced in the body are called endogenous.

Energetic particle precipitation (EPP): Precipitation of a group of highly energetic electrons, protons, neutrons, and ions that are accelerated into the atmosphere through various heliophysical and geomagnetic processes. They enter the atmosphere mainly in the vicinity of the geomagnetic poles. When energetic particles enter the atmosphere they ionize and dissociate atmospheric constituents, resulting in the formation of reactive nitrogen oxides. EPPs have been shown to contribute up to 10% of the stratospheric NO_x budget and up to 40% of the polar stratospheric NO_x budget. Once in the stratosphere, NO_x produced by EPPs (EPP-NO_x) interferes with catalytic cycles involving ozone (O_3). Theoretically, changes in O_3 can also lead to changes in temperature and winds, which means that EPPs have the potential to impact climate.

Gaussian-resampled, inverse-weighted McInerny et al. (GRIWM): Dating method for estimating the probability of extinction by using an approach that weighs observations inversely according to their temporal distance from the last observation of a species' confirmed occurrence. For dates with associated radiometric errors it is able to sample individual dates from an underlying fossilization probability distribution.

Geomagnetic excursions: Excursions represent a significant, but short-lived, change of direction of the Earth's magnetic field, and are apparently manifested globally. Intervals of constant polarity are punctuated by geomagnetic excursions where magnetic directions depart from the usual geocentric axial dipole, and when adequately recorded, achieve the opposite polarity direction for a short time. Excursions have been recorded in both volcanic and

sedimentary records. These directional aberrations typically have durations of a few thousand years, or less than 1 kyr in some cases, and are characterized by a decrease in strength of the main axial dipole.

Halons: a group of hydrocarbon compounds in which some hydrogen atoms are replaced by bromine and fluorine atoms, and sometimes also chlorine. Halons are nonconductors of electricity and may be utilized in fighting fires in ignitable liquids and most solid flammable materials. Halons in the atmosphere are responsible for ozone depletion, and contribute to greenhouse warming.

Haplogroup: group of individuals sharing a common ancestor identidfied by DNA sequences defined by shared mutations and which tend to show regional specificity. In human genetics, the most commonly studied haplogroups are Y-chromosome (Y-DNA) haplogroups and mitochondrial DNA (mtDNA) haplogroups, each of which can be used to describe genetic populations.

Haplotype: A group of genes in the chromosome of an organism that are inherited together, because of genetic linkage from a single parent. The word "haplotype" is derived from the word "haploid," that describes cells with only one set of chromosomes, and from the word "genotype," which refers to the genetic makeup of an organism.

Heinrich Stadial (HS) 4: A Heinrich event is a natural phenomenon occurring during a period known as Marine Isotops Stage 3 (about 59-27 ka BP). Large icebergs containing rock mass eroded by the glaciers break off from glaciers and traverse the North Atlantic, as they melted this material was deposited on the sea floor as ice rafted debris (IRD). One of the strongest HS is the number 4 originated around 40 ka BP.

Isothermal remanent magnetization (IRM): IRM is an artificial (usually laboratory acquired) remanent magnetization acquired by applying a strong direct field to a ferromagnetic (*sensu lato*) material. It is a useful parameter used for detection of magnetic minerals with high coercivity such as hematite or goethite.

Late Quaternary Extinction (LQE): Widespread extinction of large terrestrial mammals (megafauna) during the Late Quaternary, observed in the Americas, Europe, Africa, Asia and Australia. As the ages of extinction have become better constrained, the timing of these extinctions has become focused in the vicinity of 40 ka and 13 ka.

Ligand-binding: Intermolecular interactions occurring between or among proteins, nucleic acids, or small molecules. The interaction of ligands with their binding sites are often characterized in terms of a binding affinity. In general, high-affinity ligand binding occurs from greater intermolecular force between the ligand and its receptor, whereas low-affinity ligand binding involves less intermolecular force between the ligand and its receptor.

Luminescence age dating: refers to a group of dating methods based on the determining of how long ago mineral grains were last exposed to sunlight. The techniques include optically stimulated luminescence (OSL), infrared stimulated luminescence (IRSL), and thermoluminescence dating (TL). It is useful to geologists and archaeologists who want to know the age of a particular event. Sediments and soils contain traces of radioactive isotopes such as potassium, uranium, thorium, and rubidium. The ionizing radiation emitted during the decay of these elements is absorbed and trapped by quartz and potassium feldspar grains occurring in the sediment. Stimulating these mineral grains using either light (blue or green for OSL; infrared for IRSL) or heat (for TL) produces a luminescence signal emitted as stored unstable electron energy, the intensity of which varies depending on the amount of radiation absorbed during burial, and specific properties of the mineral.

Mediterranean sapropel S7: The sediments of the Mediterranean (central-eastern) are characterized by the presence of organic–rich (>2% organic carbon) layers called sapropels. They were deposited during periods of reduced oxygenation related to increasing riverine input occurring in correspondence with peaks in solar insolation. Each peak has been

numbered starting from the youngest (S1; 8-10 ka) and the sapropel S7 occurred around 190 ka.

Melanocyte homeostasis: The maintenance of systems within a cell as conditions change is called homeostatic regulation, and melanocyte (a mature melanin-forming skin cell) homeostasis is a paradigm for understanding the formation of melanoma.

Mitochondria: Mitochondria are part of a eukaryote cell found in the cytoplasm. They oxidise glucose to provide energy for the cell trough the creation of a molecule, called adenosine triphosphate that cells use as an energy source.

Mitochondrial DNA (mtDNA): Mitochondria are tiny organelles that live in the cytoplasm of cells, called mitochondria. Each cell contains thousands of mitochondria with its own small circle of DNA, a reminder of their distant bacterial ancestry. MtDNA is not located in the cell nucleus and in most species, including humans, it is inherited solely from the mother and is not subject to genetic recombination during meiosis. Therefore it remains unchanged from generation to generation. Human mtDNA was the first significant part of the human genome to be sequenced. Since animal mtDNA evolves faster than nuclear genetic markers, it represents a pillar of phylogenetics and evolutionary biology. It also makes possible an examination of the affinity of populations, and so has become important in anthropology and biogeography.

Mitochondrial Eve. Analyses of the mitochondrial DNA of living humans have shown that we descend from a common female ancestor that has been dated to about 200 ka. This woman has been named "Eve" or "Mitochondrial Eve" after a journalist's confusing reference to the unrelated biblical story of the first woman being created by God from Adam's rib. ("The man called his wife Eve ["life"], because she was the mother of all who live." Genesis 3:20)

Mitohormesis: Mitohormesis, known also as mitochondrial hormesis, is a particular form of hormesis that is a non-linear response to potentially harmful substances. Mitochondrial function often results in excessive production of reactive oxygen species (ROS) that are responsible of many chronic diseases. However, moderate levels of mitochondrial ROS, can protect against chronic disease by stimulating mitochondrial capacity and endogenous antioxidant defence. This phenomenon is called mitohormesis.

Mousterian tool industry: The predominant industry of the Middle Paleolithic is termed Mousterian, named for its type-site Le Moustier, in Dordogne, France. Mousterian industry is the tool culture traditionally associated with Neanderthal man in Europe, western Asia, and northern Africa. Mousterian tools disappeared abruptly from Europe with the passing of Neanderthal man.

Natural remanent magnetization (NRM): The magnetic remanence carried by rocks or sediments before the laboratory demagnetization or magnetization treatments. The NRM of a rock or sediment is usually represented by multiple magnetization components acquired through its geologic history. Thermal or alternating field laboratory treatments are usually necessary to identify the primary remanence acquired at the time of the rock formation or sediment deposition.

Pedigree-based substitution rate: A method to estimate mutation rate by comparing the mtDNA sequences of a sample of parent/offspring pairs or analyzing mtDNA sequences of individuals from a deep-rooted (well established) genealogy. The number of new mutations in the sample is counted and divided by the total number of parent-to-child DNA transmission events to calculate a mutation rate.

Perissodactyla: Order of odd-toed ungulates, hoofed animals that bear most of their weight on a single toe including horses, zebras, rhinoceroses and tapirs.

Peto's paradox: Peto's paradox, named after Richard Peto, is the observation that at species level, the incidence of cancer does not appear to correlate with the number of cells in

an organism (e.g., body weight). Although cell mutations are usually deleterious, the incidence of cancer is not apparently related to the body-size of the individual mammals.

Phenotypical. The observable physical or biochemical characteristics of an organism determined by genetic and environmental influences.

Phylogeny: The evolutionary history and relationships among people or groups of organisms (e.g. species or populations). These relationships can be discovered through phylogenetic methods that evaluate observed heritable traits, such as DNA sequences or morphology, using an evolutionary model for these traits. The results of these analyses represent the phylogeny (also referred to as the phylogenetic tree).

Polar-stratospheric clouds: Polar-stratospheric clouds are typically formed in the stratosphere (15-25 km altitude) at high latitudes especially in winter because they require very low temperatures. They are implicated in the formation of ozone holes because they convert benign forms of chlorine into reactive, ozone-destroying forms, and they remove gaseous nitric acid that would otherwise moderate the destructive impact of chlorine.

Quaternary: The most recent of the three periods of the Cenozoic Era in the geologic time scale. It spans the last 2.588 Myrs and is divided into two epochs: the Pleistocene (2.588 million years ago to 11.7 thousand years ago) and the Holocene (11.7 thousand years ago to present).

Reactive oxygen species (ROS): Oxygen-derived molecules that act as powerful oxidants and may form via a large number of physiologic and non-physiologic processes as a result of natural consequences of aerobic metabolism. Although these molecules play a role in the oxygen-dependent defence mechanism against bacteria, they may also be highly damaging, as they can attack biologic macromolecules, including lipids, proteins, and DNA, and lead to significant tissue damage. In normal conditions, ROS can act as immune system modulation and can activate various signal transduction pathways. ROS levels can increase dramatically during times of environmental stress (e.g., UVR or heat exposure).

Relative paleointensity (RPI): The intensity of the Earth's axial dipole field is globally coherent, and can be reconstructed in the past by studying suitable rock and sediment samples or archaeological materials. The RPI proxy in sediments usually comprises the NRM intensity normalized by the intensity of a laboratory-acquired magnetization designed to activate the same population of magnetic grains that carry the NRM, thus compensating for variations in concentration of NRM-carrying grains through the sedimentary section. The laboratory-applied normalizers are typically anhysteretic remanent magnetization (ARM) and/or isothermal remanent magnetization (IRM).

Signor-Lipps effect: The first and last occurrence of a taxon will never be accurately recorded in the fossil record because of the inherent incompleteness of the record.

Sclerophyll vegetation: Type of vegetation characterized by hard, leathery, evergreen foliage well adapted to prevent moisture loss. Broad-leaved sclerophyll vegetation, including species such as holly (Ilex), is known as Mediterranean vegetation because it develops in regions with a Mediterranean climate - hot, dry summers and mild, wet winters. Pines are examples of narrow-leaved sclerophyll vegetation.

Solar proton events (SPE): A SPE or "proton storm", occurs when particles (mostly protons) emitted by the Sun are accelerated either close to the Sun during a flare or in interplanetary space by coronal mass ejection (CME). Solar protons normally have insufficient energy to penetrate the Earth's protective magnetosphere. However, during unusually strong flares, protons can be produced with sufficient energies to penetrate the Earth's magnetosphere and ionosphere around the poles. They can pass trough the Earth's magnetic field and cause ionization in the ionosphere. The effect is analogous to an auroral event, except that protons instead of electrons are involved. Energetic protons represent a significant radiation hazard to spacecraft and astronauts.

The time to the most recent common ancestor (TMRCA): Time to the most recent individual from which an entire organism is directly descended. The term is used in reference to the ancestry of groups of genes (haplotypes) or species.

TP53 (p53) gene: Tumour protein 53 is a protein-coding gene that acts as a tumour suppressor for many tumour types, and induces growth arrest or apoptosis depending on physiological circumstances and cell type. The TP53 gene is responsible for instructions to create a protein called tumour protein p53. This protein acts as a tumour suppressor, which means that it regulates cell division by keeping cells from growing and dividing (proliferating) too fast or in an uncontrolled way. The p53 protein is found in the nucleus of cells throughout the body, where it attaches (binds) directly to DNA. If the DNA in a cell is damaged by agents such as toxic chemicals, radiation or UVR, this protein plays a critical role as to whether the DNA can be repaired or the damaged cell will self-destruct (undergo apoptosis). If it is possible to repair the DNA, p53 activates other genes to fix the damage. On the other hand, this protein prevents the cell from dividing and signals it to undergo apoptosis. By stopping cells with mutated or damaged DNA from dividing, p53 helps prevent tumour development.

Tryptophan: Tryptophan is a α-amino acid that is used in the biosynthesis of proteins. Many animals (including humans) cannot synthesize tryptophan: they obtain it through their diet. Tryptophan is among the less common amino acids found in proteins, but it has critical structural and functional roles.

Virtual axial dipole moment (VADM): Intensity of an imaginary axial (along the Earth's rotation axis) centric (located in the centre of the Earth) dipole that would produce the estimated magnetic field reconstructed from paleomagnetic data. The reconstruction is virtual because the VADM is an approximation of a geocentric axial dipole moment.

Xenobiotics: A xenobiotic is a chemical substance within an organism that is foreign to the biological system, and not naturally produced or expected to be present within the organism. It can also cover substances that are present in much higher concentrations than usual. The term is often used in the context of pollutants, and their effect on biota.

Y-chromosome: one of the two sex chromosomes in humans (the other is the X chromosome) and most mammals. The Y chromosome occurs in males, who have one X and one Y chromosome, while females have two X chromosomes. The Y chromosome contains genes that provide instructions for making proteins. Because only males have the Y chromosome, the genes in this chromosome are involved in male sex determination and development. The Y chromosome represents almost 2 % of the total DNA in male cells.

Figure 1.

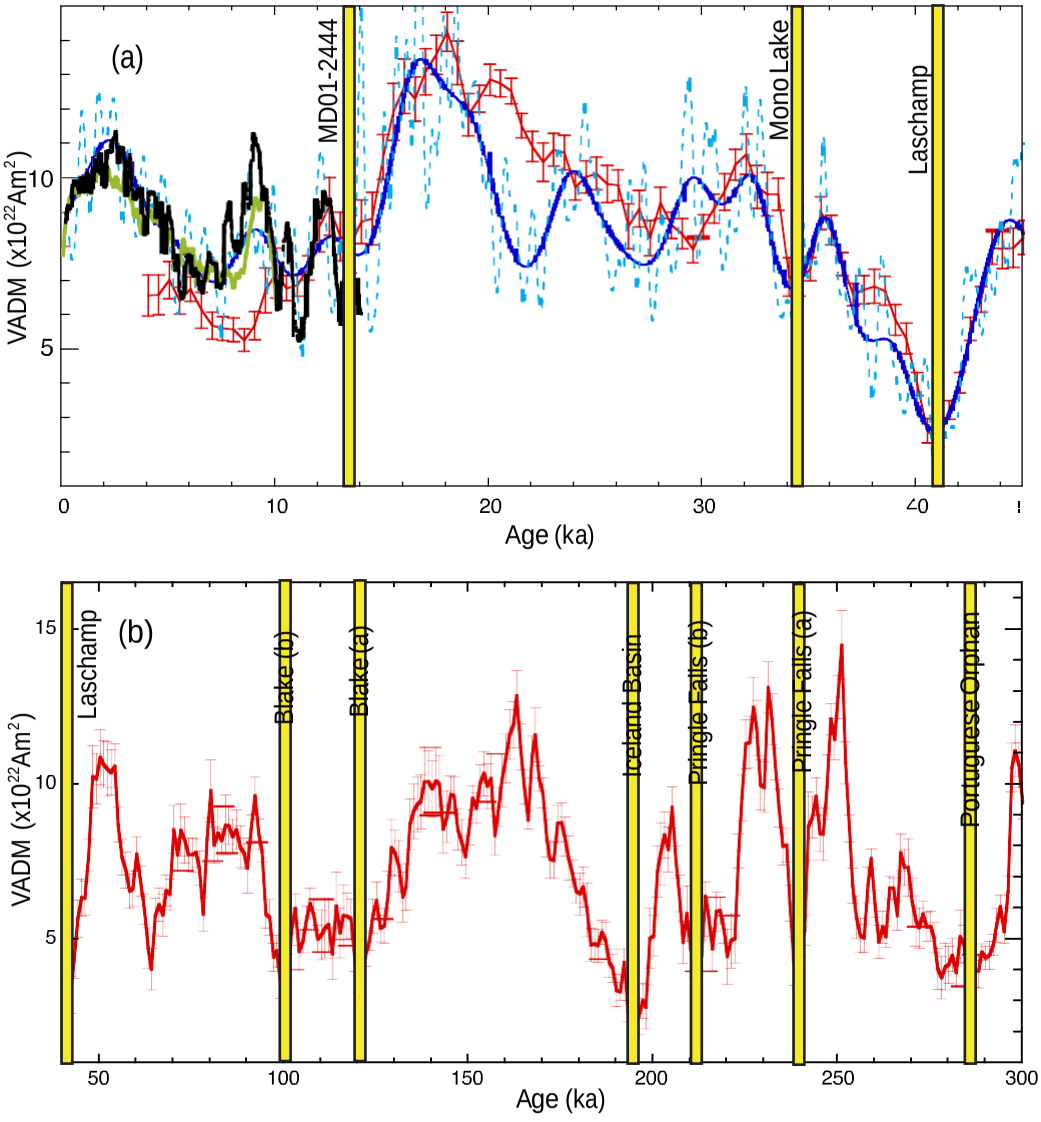
(a)
MD01-2444
Mono Lake
Laschamp
VADM (x10^22Am^2)
5
10
0
10
20
30
Age (ka)
(b)
Laschamp
Blake (b)
Blake (a)
Iceland Basin
Pringle Falls (b)
Pringle Falls (a)
Portuguese Orphan
VADM (x10^22Am^2)
5
10
15
50
100
150
200
250
300
Age (ka)

Figure 2.

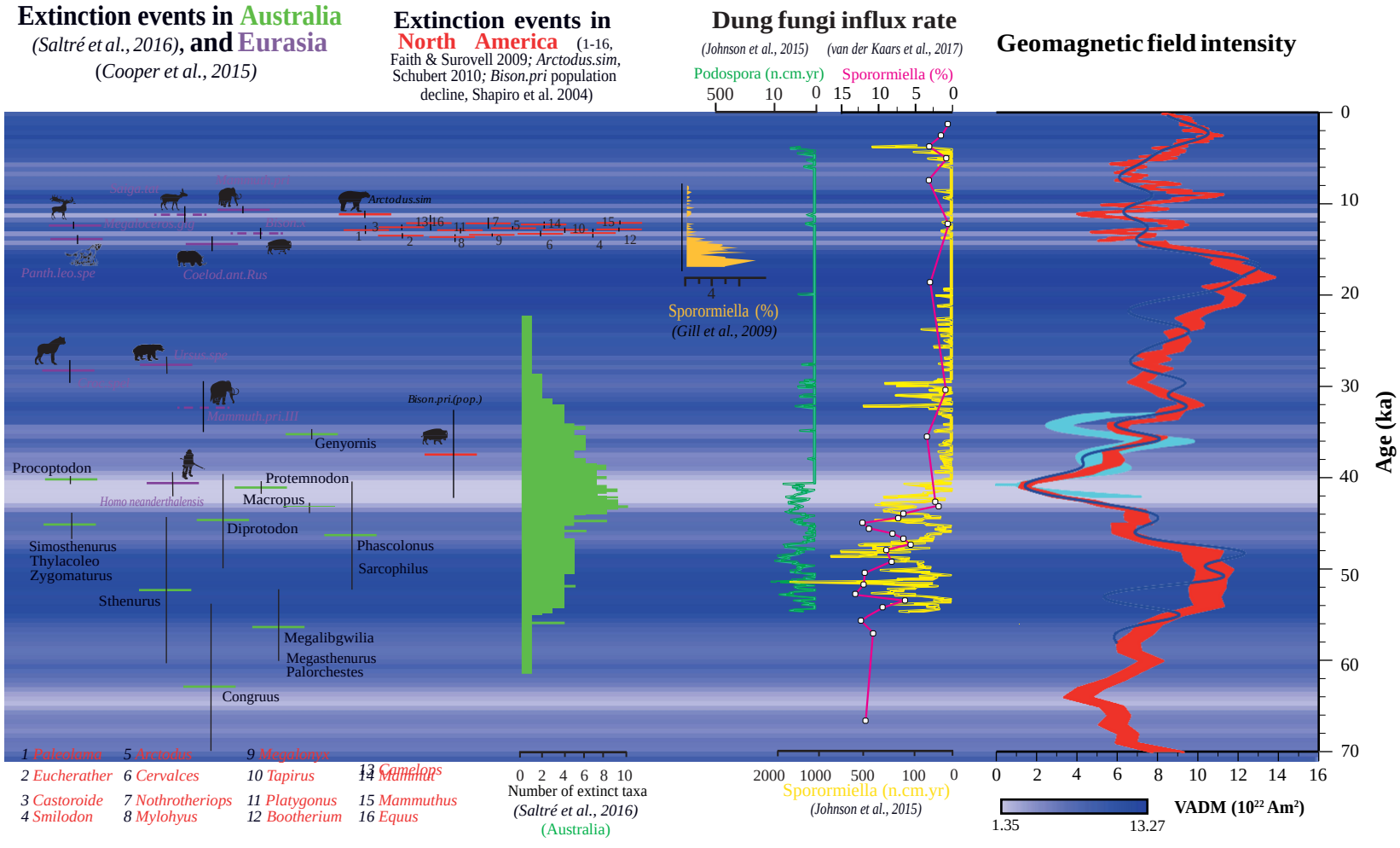
Extinction events in Australia
(Saltré et al., 2016), and Eurasia
(Cooper et al., 2015)
Extinction events in North America (1-16, Faith & Surovell 2009; Arctodus.sim, Schubert 2010; Bison.pri population decline, Shapiro et al. 2004)
Dung fungi influx rate
(Johnson et al., 2015) (van der Kaars et al., 2017)
Podospora (n.cm.yr)
Sporormiella (%)
Geomagnetic field intensity
Arctodus.sim
Panth.leo.spe
Coelod.ant.Rus
Ursus.spe
Mammuth.pri.III
Bison.pri.(pop.)
Sporormiella (%)
(Gill et al., 2009)
Genyornis
Procoptodon
Homo neanderthalensis
Protemnodon
Macropus
Diprotodon
Simosthenurus
Thylacoleo
Zygomaturus
Phascolonus
Sarcophilus
Sthenurus
Megalibgwilia
Megasthenurus
Palorchestes
Congruus
1 Paleolama
2 Eucherather
3 Castoroide
4 Smilodon
5 Arctodus
6 Cervalces
7 Nothrotheriops
8 Mylohyus
9 Megalonyx
10 Tapirus
11 Platygonus
12 Bootherium
13 Camelops
14 Mammut
15 Mammuthus
16 Equus
Number of extinct taxa
(Saltré et al., 2016)
(Australia)
Sporormiella (n.cm.yr)
(Johnson et al., 2015)
VADM (10^22 Am^2)
1.35
13.27
Age (ka)

Figure 3.

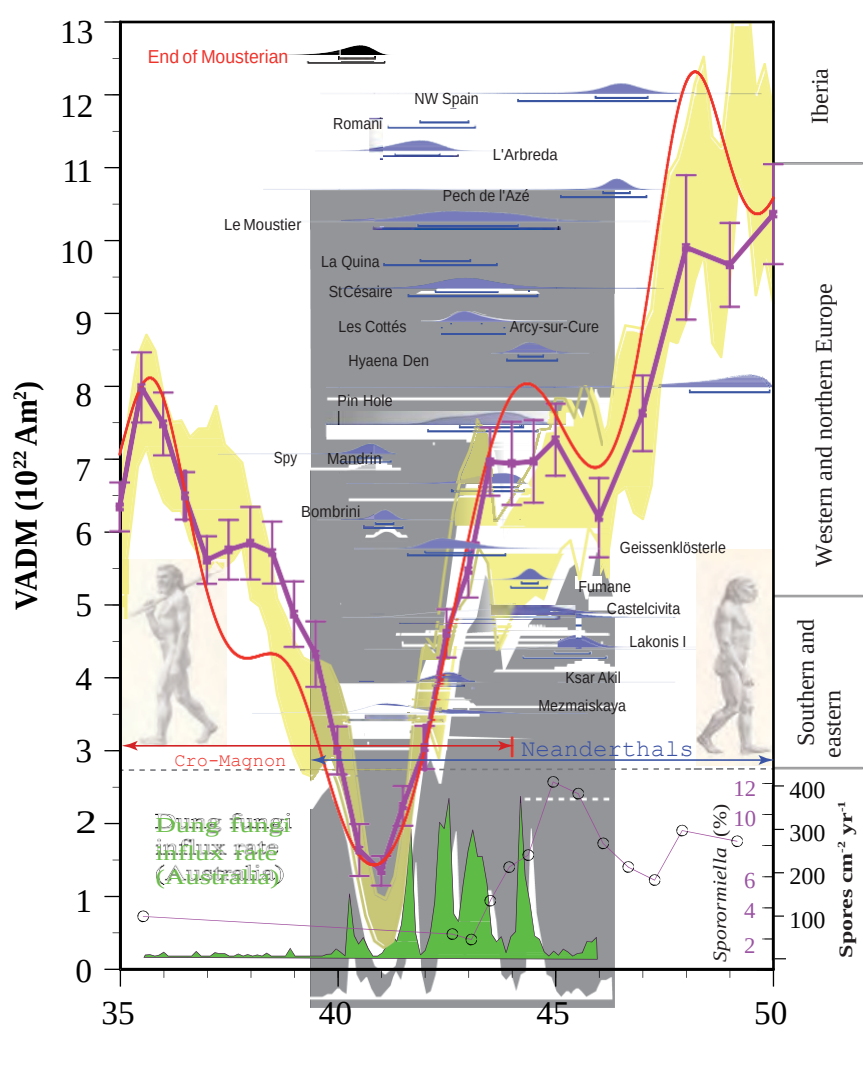
VADM (10^{22} Am^2)
13
12
11
10
9
8
7
6
5
4
3
2
1
0
35
40
45
50
End of Mousterian
NW Spain
Romaní
L'Arbreda
Pech de l'Azé
Le Moustier
La Quina
StCésaire
Les Cottés
Arcy-sur-Cure
Hyaena Den
Pin Hole
Spy
Mandrin
Bombrini
Geissenklösterle
Fumane
Castelcivita
Lakonis I
Ksar Akil
Mezmaiskaya
Cro-Magnon
Neanderthals
Dung fungi influx rate (Australia)
Sporormiella (%)
Spores cm^{-2} yr^{-1}
Iberia
Western and northern Europe
Southern and eastern

AGE (ka)

Figure 4.

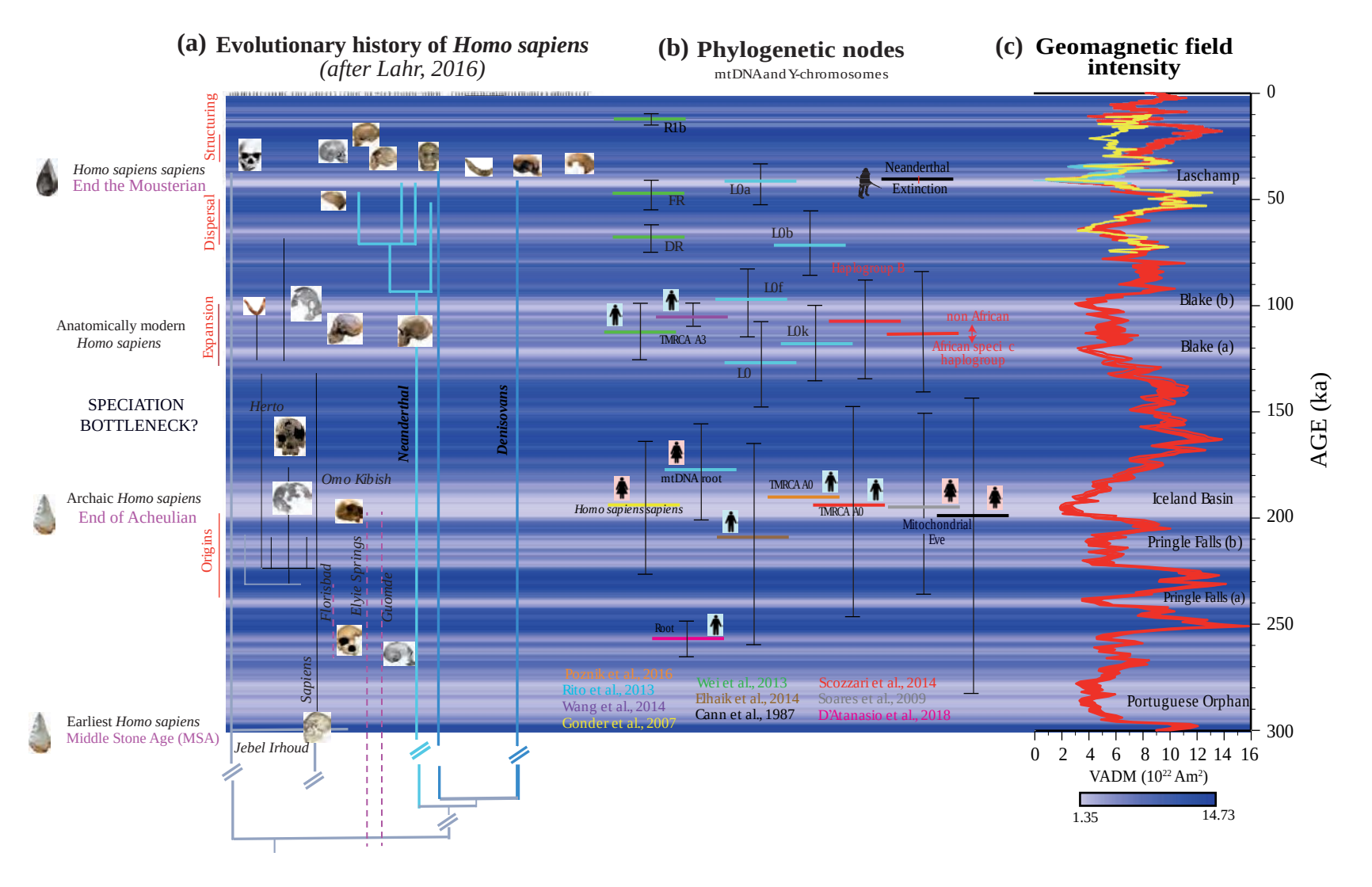
(a) Evolutionary history of Homo sapiens
(after Lahr, 2016)
(b) Phylogenetic nodes
mtDNA and Y-chromosomes
(c) Geomagnetic field intensity
Structuring
Dispersal
Expansion
Origins
Homo sapiens sapiens
End the Mousterian
Anatomically modern
Homo sapiens
SPECIATION
BOTTLENECK?
Archaic Homo sapiens
End of Acheulian
Earliest Homo sapiens
Middle Stone Age (MSA)
Herto
Omo Kibish
Florisbad
Elyie Springs
Guomde
Sapiens
Jebel Irhoud
Neanderthal
Denisovans
R1b
FR
DR
L0a
L0b
L0f
L0k
L0
TMRCA A3
Haplogroup B
non African
African specific
haplogroup
Neanderthal
Extinction
mtDNA root
Homo sapiens sapiens
TMRCA A0
TMRCA A0
Mitochondrial
Eve
Root
Pozmik et al., 2016
Rito et al., 2013
Wang et al., 2014
Gonder et al., 2007
Wei et al., 2013
Elhaik et al., 2014
Cann et al., 1987
Scozzari et al., 2014
Soares et al., 2009
D'Atanasio et al., 2018
Laschamp
Blake (b)
Blake (a)
Iceland Basin
Pringle Falls (b)
Pringle Falls (a)
Portuguese Orphan
AGE (ka)
0
50
100
150
200
250
300
0 2 4 6 8 10 12 14 16
VADM (10^22 Am^2)
1.35
14.73